Geochimica et Cosmochimica Acta 404 (2025) 53–71

Contents lists available at ScienceDirect

Geochimica et Cosmochimica Acta

journal homepage: www.elsevier.com/locate/gca

Spatial evidence of cryptic methane cycling and methylotrophic metabolisms along a land–ocean transect in salt marsh sediment

Sebastian J.E. Krause [a,1,*], Rebecca Wipfler [c], Jiarui Liu [a], David J. Yousavich [a], DeMarcus Robinson [b], David W. Hoyt [d], Victoria J. Orphan [c], Tina Treude [a,*]

[a] Department of Earth, Planetary, and Space Sciences, University of California, Los Angeles, CA 90095, USA
[b] Department of Atmospheric and Ocean Sciences, University of California, Los Angeles, CA 90095, USA
[c] Division of Geological and Planetary Sciences, California Institute of Technology, Pasadena, CA 91125, USA
[d] Pacific Northwest National Laboratory Environmental and Molecular Sciences Division, Richland, WA 99352, USA

ARTICLE INFO

Associate editor: Damien Troy Maher

Keywords:
Sulfate reduction
Iron reduction
Anaerobic oxidation of methane
Methanogenesis
Mono-methylamine
Sulfate-reducing bacteria
Methanogenic archaea
Methanotrophic archaea

ABSTRACT

Methylotrophic methanogenesis in the sulfate-rich zone of coastal and marine sediments couples with anaerobic oxidation of methane (AOM), forming the cryptic methane cycle. This study provides evidence of cryptic methane cycling in the sulfate-rich zone across a land–ocean transect of four stations–two brackish, one marine, and one hypersaline–within the Carpinteria Salt Marsh Reserve (CSMR), southern California, USA. Samples from the top 20 cm of sediment from the transect were analyzed through geochemical and molecular (16S rRNA) techniques, in-vitro methanogenesis incubations, and radiotracer incubations utilizing ^{35}S-SO_4, ^{14}C-mono-methylamine, and ^{14}C-CH_4. Sediment methane concentrations were consistently low (3 to 28 μM) at all stations, except for the marine station, where methane increased with depth reaching 665 μM. Methanogenesis from mono-methylamine was detected throughout the sediment at all stations with estimated CH_4 production rates in the sub-nanomolar to nanomolar range per cm^3 sediment and day. 16S rRNA analysis identified methanogenic archaea (*Methanosarcinaceae*, *Methanomassiliicoccales*, and *Methanonatronarchaeacea*) capable of producing methane from methylamines in sediment where methylotrophic methanogenesis was found to be active. Metabolomic analysis of porewater showed mono-methylamine was mostly undetectable (<3 μM) or present in trace amounts (<10 μM) suggesting rapid metabolic turnover. In-vitro methanogenesis incubations of natural sediment showed no linear methane buildup, suggesting a process limiting methane emissions. AOM activity, measured with ^{14}C-CH_4, overlapped with methanogenesis from mono-methylamine activity at all stations, with rates ranging from 0.03 to 19.4 nmol cm^{-3} d^{-1}. Geochemical porewater analysis showed the CSMR sediments are rich in sulfate and iron. Porewater sulfate concentrations (9–91 mM) were non-limiting across the transect, supporting sulfate reduction activity (1.5–2,506 nmol cm^{-3} d^{-1}). Porewater sulfide and iron (II) profiles indicated that the sediment transitioned from a predominantly iron-reducing environment at the two brackish stations to a predominantly sulfate-reducing environment at the marine and hypersaline stations, which coincided with the presence of phyla (Desulfobacterota) involved in these processes. AOM activity overlapped with sulfate reduction and porewater iron (II) concentrations suggesting that AOM is likely coupled to sulfate and possibly iron reduction at all stations. However, 16S rRNA analysis identified anaerobic methanotrophs (ANME-2) only at the marine and hypersaline stations while putative methanogens were found in sediment across all stations. In one sediment horizon at the marine station, methanogen families (*Methanosarcinaceae*, *Methanosaetaceae*, *Methanomassiliicoccales*, and *Methanoregulaceae*) and ANME 2a,2b, and 2c groups were found together. Collectively, our data suggest that at the brackish stations methanogens alone may be involved in cryptic methane cycling, while at the marine and hypersaline stations both groups may be involved in the process. Differences in rate constants from incubations with ^{14}C-labeled methane and mono-methylamine suggest a non-methanogenic process oxidizing mono-methylamine to inorganic carbon, likely mediated by sulfate-reducing bacteria. Understanding the potential competition of sulfate reducers with methanogens for mono-methylamine needs further investigation as it might be another important process responsible for low methane emissions in salt marshes.

* Corresponding authors.
E-mail addresses: sjkrause@ucsb.edu, sjkrause12@gmail.com (S.J.E. Krause), ttreude@g.ucla.edu (T. Treude).
[1] Present address: Earth Research Institute, 6832 Ellison Hall, University of California Santa Barbara, Santa Barbara, CA 93106-3060, USA.

https://doi.org/10.1016/j.gca.2025.07.019
Received 17 December 2024; Accepted 21 July 2025
Available online 23 July 2025

1. Introduction

Methane is the simplest and most abundant organic molecule in the atmosphere and is about 25–30 times more potent than carbon dioxide as a greenhouse gas (IPCC, 2021). Since pre-industrial technological advancement, methane concentrations in the atmosphere have nearly tripled from 722 ppb to 1912 ppb in 2022 (Saunois et al., 2025; Wang et al., 2024). Natural wetlands are broadly characterized into freshwater and coastal wetlands. Both ecosystems contain organic-rich sediment that could sustain microbial methanogenesis. However, coastal wetlands, such as mangroves, salt marshes and seagrasses combined, emit far less methane into the atmosphere (0.47–1.41 Tg CH_4 yr^{-1}) (Rosentreter et al., 2021; Rosentreter et al., 2023) than their freshwater counter parts (159 Tg CH_4 yr^{-1}) (Saunois et al., 2025). The lower methane emission is due to the presence of sulfate which enters coastal wetlands via marine seawater inflow and mixes with freshwater inflows creating distinct salinity gradients in the overlying water (Cui et al., 2024; Reddy et al., 2022). Salinity in the sediment of coastal wetlands is mostly driven by daily tidal influence (del Pilar Alvarez et al., 2015; Gardner, 2007; Li et al., 2023; Moffett et al., 2010; Reddy et al., 2022) but also wetland geomorphology, sediment characteristics, climate conditions (Montalto et al., 2006), evapotranspiration, bioturbation (Cao et al., 2012; Carol et al., 2011; Li et al., 2023), and anthropogenic alterations (Carol et al., 2012). The sulfate that enters wetlands' sediment porewater, supports microbial sulfate reduction and thereby suppresses competitive methanogenesis pathways (hydrogenotrophic and acetoclastic) (Jørgensen, 2000; Kristjansson et al., 1982; Lovley and Klug, 1986; Oremland et al., 1982; Oremland and Polcin, 1982; Winfrey and Ward, 1983). As a result, methane tends to buildup in deeper anoxic sediment below the sulfate penetration depth. In the lower portion of the sulfate reduction zone, where the concentration of sulfate is decreasing and overlaps with increasing methane concentration is the sulfate methane transition zone (SMTZ), where anaerobic oxidation of methane (AOM) occurs (Gao et al., 2022; Hinrichs and Boetius, 2002; Knittel and Boetius, 2009; Lapham et al., 2024; Reeburgh, 2007; Zhao et al., 2024). In the SMTZ, AOM oxidizes methane with sulfate as the electron acceptor and has been shown to consume up to 96% of methane before reaching the water column within coastal wetland sediment (La et al., 2022). The process is typically mediated by a consortium of anaerobic methane-oxidizing archaea (ANME) and sulfate-reducing bacteria (Boetius et al., 2000; Hinrichs and Boetius, 2002; Knittel and Boetius, 2009; Michaelis et al., 2002; Orphan et al., 2001b; Reeburgh, 2007).

Although sulfate reduction outcompetes methanogenesis for hydrogen and acetate in the sulfate reduction zone above the SMTZ, methylated substrates such as methylsulfides, methanol and methylamines, are known to be non-competitive substrates for methanogenesis of the methylotrophic pathways (Krause et al., 2023; Krause and Treude, 2021; Lovley and Klug, 1986; Maltby et al., 2016; Oremland and Taylor, 1978; Zhuang et al., 2016; Zhuang et al., 2018). Thus, methylotrophic methanogenesis activity has been shown to occur within the sulfate-reducing zone in various aquatic environments, including coastal wetland environments (Bueno de Mesquita et al., 2023; Dong et al., 2024; Krause and Treude, 2021; Oremland et al., 1982; Oremland and Polcin, 1982; Reddy et al., 2022; Schorn et al., 2022; Yuan et al., 2019). However, despite the methylotrophic methanogenesis activity, methane concentrations are by several orders of magnitude lower above the SMTZ compared to deeper sediments where sulfate is depleted (Barnes and Goldberg, 1976; Beulig et al., 2018; Krause et al., 2023; Krause and Treude, 2021; Wehrmann et al., 2011). This low level of methane is controlled by concurrent methylotrophic methanogenesis and AOM activity which is now referred as the cryptic methane cycle, and has been detected in marine and coastal wetland sediment (Krause et al., 2023; Krause and Treude, 2021; Xiao et al., 2018; Xiao et al., 2017).

Important questions remain about how methane is cycled in coastal wetlands across spatial gradients and electron acceptor availability. Moreover, the microbial communities, that may be involved directly or indirectly with the cryptic methane cycle have not been identified. Coastal wetlands are ideal geographical features to study these questions because of their unique hydrology where freshwater and marine sources interact creating natural gradients between salinity and terrestrial input, which potentially affects the availability of important electron acceptors (e.g., sulfate and iron (III)) and the related microbial communities that drive cryptic methane cycling. Therefore, it is crucial to investigate the biogeochemical trends, the metabolic activity of methanogenesis, AOM and sulfate reduction, as well as characterize the microbial communities along a natural salinity gradient of coastal wetlands.

The primary objective is to study cryptic methane cycling along a spatial transect following a natural salinity gradient in a California coastal wetland, the Carpinteria Salt Marsh Reserve (CSMR). Thereby, we aim to elucidate the availability of electron acceptors that drive AOM, and to characterize the microbial communities that are responsible for cryptic methane cycling. In the following study we will show concurrent activities of methanogenesis and AOM, along with potential microbial communities involved, within sulfate-rich sediment across the CSMR land–ocean transect, which strongly suggest active cryptic methane cycling. In addition, our data point to the existence of non-methanogenic anaerobic methylotrophic metabolism alongside the cryptic methane cycle.

2. Materials and methods

2.1. Study area and field study

The field site for this study is the Carpinteria Salt Marsh Reserve (CSMR), which is located about 15 km east of Santa Barbara, California USA and is part of the University of California Natural Reserve system. Within the CSMR, three freshwater streams flow from the North to the South and open into the Pacific Ocean (Fig. 1). Seawater does infiltrate the CSMR through daily tidal fluxes and mixes with freshwater that enters the CSMR from the North. The mixing results in a natural salinity gradient in the surface waters during low tide. In July of 2019, sediment samples for this study were collected from a total of four stations (three inside connected creeks and one inside an isolated pool) within the CSMR along a land–ocean, i.e., North-South, transect featuring differences in salinity in the overlying water. Stations were picked based on accessibility and the salinity of the overlying water during low tide, measured in the field with a hand-held refractometer. The stations include brackish low (BL, 7 PSU, 34°24′12.6″N, 119°32′06.8″W), brackish high (BH, 15 PSU, 34°24′10.1″N, 119°32′01.2″W), marine (M, 35 PSU, 34°23′56.3″N, 119°32′12.0″W), and hypersaline (HP, 139 PSU, 34°23′56.1″N, 119°32′10.2″W) conditions. The hypersaline conditions are linked to an isolated, evaporative pool, which has been studied previously (Krause and Treude, 2021; Liu et al., 2025).

The top 15 to 20 cm of sediment at each station was collected in large (10 cm i.d.) and small (2.6 cm i.d.) polycarbonate push cores. Push cores were carefully inserted into sediment by hand including approximately 5 cm overlying water. Large push cores were inserted approximately 20 cm from each other, while small push cores were inserted approximately 15 cm from each other to provide sufficient space for push core extraction. Sediment surrounding the push cores was carefully removed to place a metal plate under the bottom to safely extract the push cores. Any air headspace within the push cores were filled bubble-free with overlying-water from the station location along the creek or hypersaline pool and sealed with rubber stoppers and electrical tape. Sediment push cores were transported to the home laboratory on the same day, stored in the dark at room temperature and processed within 1 d to 1 wk of collection, depending on the analysis type (see 2.2 – 2.7).

2.2. Porewater geochemistry and solid phase analysis

One day after collection, one large push core from each station was selected for porewater geochemistry analysis. At all stations the top

layer of the sediment was sliced at 1.5 cm followed by 1-cm increments due to natural slopes found at the sediment surfaces during the time of sampling. All sediment was sliced under a constant flow of argon gas to minimize oxidation of oxygen-sensitive substrates. The sediment sections were transferred to pre-argon flushed 50 mL centrifuge vials and centrifuged at 4300 *g* for 20 mins. Immediately after centrifugation, the separated porewater was analyzed spectrographically for dissolved sulfide according to Cline (1969) and iron (II) according to Grasshoff et al. (1999) using a Shimadzu UV-Spectrophotometer (UV–1800) equipped with a sipper unit. The remaining porewater was frozen (−30°C) and later measured for dissolved porewater sulfate and chloride concentrations. Porewater sulfate and chloride was determined using an ion chromatograph (Metrohm 761) (Dale et al., 2015). Analytical precision of these measurements was <1% based on repeated analysis of IAPSO seawater standards. Absolute detection limit of sulfate was 1 μM, which corresponds to 30 μM in the undiluted sample. Porewater salinity at each station was calculated from chlorinity using Knudson's equation (Salinity = 1.805 * Chlorinity) assuming that the major ionic ratios in the porewater and in seawater are similar (Knudsen, 1901). One mL of porewater was subsampled for the determination of methylamine concentrations and other methanogenic substrates (see section 2.4).

For methane concentrations, porosity/density, solid-phase carbon/nitrogen, and molecular analysis, a separate large push core from each station, the top 1.5 cm was sliced followed by 1-cm increments because of natural slopes at the sediment surface found at the time of sampling. For methane concentrations, 2 mL of sediment at each interval was subsampled using a 3 mL cut-off plastic syringe and transferred to a 12 mL glass serum vial filled with 5 mL of 5% NaOH and sealed with grey butyl rubber stoppers. Headspace methane concentrations were later determined using a Shimadzu gas chromatograph (GC–2014) equipped with a packed Haysep D column and flame ionizer detector. The column was heated to 80°C and ultra-high pure helium was used as the carrier gas, set to 12 mL per minute. A methane standard (Scotty Analyzed Gases) was used to calibrate for methane concentrations with a ± 5% precision.

For porosity and density, 8 mL of sediment was collected from each 1 cm layer using a 10 mL plastic cut off syringe, transferred to pre-weighed plastic 10 mL vials (Wheaton). The wet samples were then weighed and then stored at 4°C. The samples were later dried at 75°C for 72 h and then reweighed. Sediment porosity was determined by subtracting the dry sediment weight from the wet sediment weight and dividing by the total volume. Sediment density was determined by dividing the wet weight by the total volume of the sample.

Analyses for sediment total organic carbon (TOC) and total organic nitrogen (TON) were modified from Harris et al., (2001). Briefly, samples were dried up to 48 h at 50°C until the dry weight was stable and then treated with direct addition of 1 mL of 6 N HCl to dissolve carbonate minerals. These samples were then washed in triplicate with 1 mL of ultrapure water or until a neutral pH was re-established. Samples were centrifuged at 4255 *g* for 20 min, the supernatant was decanted, and vials were re-dried at 50°C. A subsample (approx. 10–15 mg) was then packed into individual 8x5 mm pressed tin capsules and sent to the University of California Davis Stable Isotope Facility for analysis using Elemental Analyzer – Isotope Ratio Mass Spectrometry. TOC and TON were calculated based on the sample peak area corrected against a reference material (alfalfa flour).

For molecular analysis, 2 sets of 3 mL of sediments were collected using a 3 mL plastic cut-off syringe into 3 mL plastic cryo vials and immediately stored at −80°C for further analysis (see section 2.9 for details).

2.3. In-vitro net methanogenesis

One week after sample collection, one large push core from each station was selected to study in-vitro methanogenesis in the natural sediments. Between 2 and 3 sediment intervals at each station were selected and subsampled for this analysis based on porewater geochemistry and solid-phase analysis (see details in Fig. 3).

Sediment subsampling was performed similarly to section 2.2. Each push core was sliced at the designated sediment layers under a constant flow of argon to minimize oxygen poisoning of anaerobic microbial communities within the sediment. Using a 3 mL plastic cut-off syringe, 10 mL sediment from each interval was transferred into triplicate sterilized, argon-flushed 60 mL glass serum vials. Vials were sealed with blue butyl rubber stoppers (Bellco Glass Inc, 20 mm diameter) and crimped with aluminum crimps. The headspace of each vial was flushed

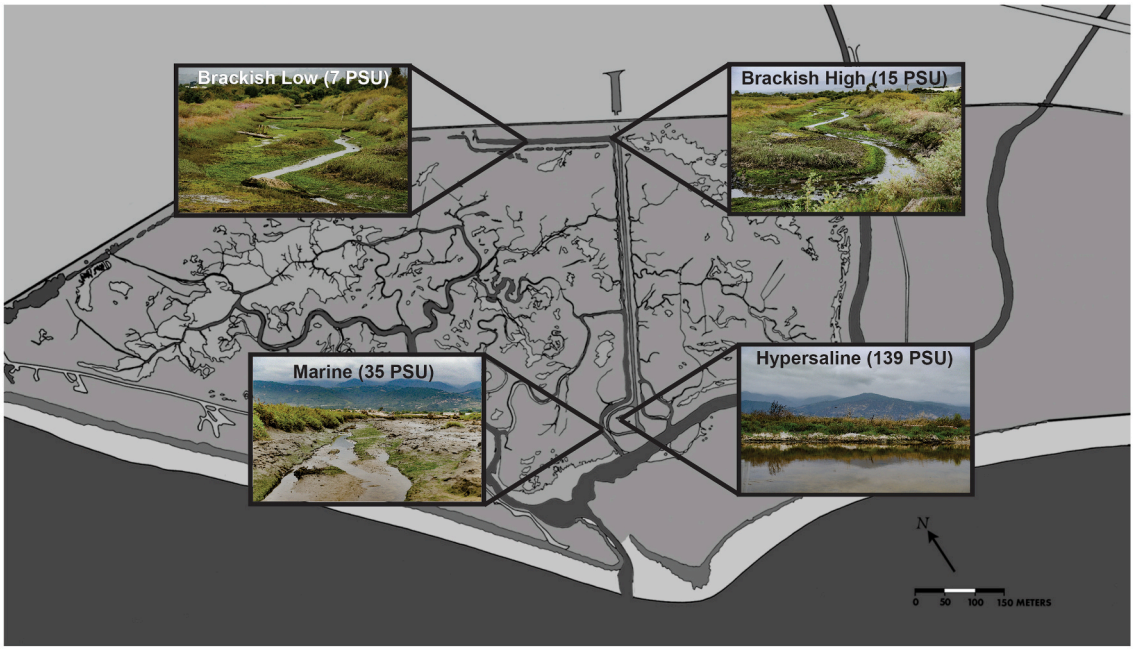

Fig. 1. Map of the Carpinteria Salt Marsh Reserve and with sampling locations along the natural salinity gradient. The Brackish Low, Brackish High and Marine stations are connected via creeks; the Hypersaline station is an evaporative isolated pool. PSU = practical salinity units.

with argon for one minute to remove oxygen. The vials were then incubated in the dark, at room temperature and monitored for 22 days. Methane concentrations in the headspace were tracked using a gas chromatograph (see section 2.2).

2.4. Metabolomic analysis

Sediment porewater concentrations of methanogenic substrates (methylamine, methanol, and acetate), were obtained from a selection of depth intervals at each station (i.e., 0–1.5 cm and 10.5–11.5 cm from the BL and BH stations and 0–1.5 cm, 10.5–11.5 cm, and 14.5–15.5 cm at the M and HP stations) by syringe-filtering (0.2 μm) 1 mL porewater into pre-combusted (350°C for 3 h) amber glass vials (1.8 mL). Samples were then closed with screw caps equipped with a PTFE septa and frozen at −80°C until analyses. Samples were analyzed at the Pacific Northwest National Laboratory, Environment and Molecular Sciences Division for metabolomic analysis using proton nuclear magnetic resonance (NMR). For details on sample preparation and analysis see section 2.4 in Krause et al. (2023).

2.5. Sulfate reduction (^{35}S-Sulfate)

Within the one day of collection, one small sediment whole round push core from each station was used to determine sulfate-reduction rates at the home laboratory. Radioactive, carrier-free $^{35}S\text{-}SO_4^{2-}$ (dissolved in MilliQ water, injection volume 10 μL, activity 260 KBq, specific activity 1.59 TBq mmol^{-1}) was injected into the whole-round cores at 1-cm intervals and incubated at room temperature and in the dark. The incubation was stopped after ~ 24 h by slicing the sediment in 1-cm intervals which were transferred to 50 mL centrifuge tubes containing 20 mL of 20% (w/w) zinc acetate solution. Each sample was thoroughly shaken to halt biological activity and then all samples were stored at −30°C until analysis. Samples were analyzed using the cold-chromium distillation method and the results from the analysis were used to calculate the sulfate reduction rates according to Kallmeyer et al. (2004).

2.6. Methanogenesis and AOM from mono-methylamine

The present study aimed to follow the methane production by methanogenesis from mono-methylamine (hereafter abbreviated MG-MMA) and the subsequent oxidation of the methane to dissolved inorganic carbon (DIC) by anaerobic oxidation of methane (hereafter abbreviated AOM-MMA) (i.e., cryptic methane cycling) in salt marsh sediments across a land-ocean transect. To find evidence of concurrent MG-MMA and AOM-MMA, one small whole round core from each station was injected with ^{14}C-mono-methylamine (^{14}C-MMA) (dissolved in water, injection volume 10 μL, activity 220 KBq, specific activity 1.85–2.22 GBq mmol^{-1}) at 1-cm intervals and stored at room temperature and in the dark for 24 h. Incubations were terminated by slicing the sediment at 1-cm intervals into 50 mL wide-mouth glass crimp vials filled with 20 mL of 5% NaOH. After transfer of the sample, vials were immediately sealed with a red butyl stopper and crimped with an aluminum crimp. Control samples were prepared by sectioning the top 5 cm of a separate whole round core from each station in 1-cm intervals into 50 mL wide mouth vials filled with 20 mL of 5% NaOH prior to radiotracer addition. Vials were shaken thoroughly for 1 min to ensure complete biological inactivity and stored upside down at room temperature till further processing. The residual ^{14}C-MMA in the liquid, the $^{14}C\text{-}CH_4$ in the headspace of the sample vials produced by MG-MMA, and the ^{14}C-TIC in the sediments as a result of AOM-MMA samples were determined by the analysis according to Krause and Treude (2021).

To account for the ^{14}C-MMA binding to mineral surfaces (Wang and Lee, 1993, 1994; Xiao et al., 2022), we determined the recovery factor (RF) for the sediment from stations BL, BH and M following the procedure of Krause and Treude (2021). In short, sediment from the 0–1, 5–6, 10–11, 14–15, and 19–20 cm intervals from the BL, BH and M stations were transferred to 250 mL Erlenmeyer flasks with 20 mL of 5% NaOH and thoroughly mixed with a magnetic stir bar and stir plate. An additional set of five 250 mL Erlenmeyer flasks were prepared with 5% NaOH and without sediment to determine the total added ^{14}C-MMA. While homogenizing the samples, ^{14}C-MMA (dissolved in water, injection volume 10 μL, activity 220 KBq, specific activity 1.85–2.22 GBq mmol^{-1}) was added to each flask prior to shaking. After all flasks containing samples were shaken for 4 h and left to rest, 100 μL of the clear supernatant was subsampled from all flasks and the radioactivity was determined by liquid scintillation. The RF was calculated by dividing the radioactivity of samples containing sediment over the radioactivity of samples without sediment. For the HP station, the RF factor previously determined by Krause and Treude (2021) was applied.

Estimates of metabolic rates of MG-MMA and AOM-MMA were calculated from the results of the ^{14}C-MMA incubations. Natural concentrations of mono-methylamine in the sediment porewater were detectable (>3 μM) but were below the quantification limit (10 μM) (See section 3.1.5). To enable rate calculations for MG-MMA (Eq. (1)), we assumed an MMA concentration of 3 μM for all samples, i.e., the detection limits of the NMR analysis.

$$\text{MG-MMA} = \frac{a_{CH_4} + a_{TIC}}{a_{CH_4} + a_{TIC} + \left[\frac{a_{MMA}}{RF}\right]} * [MMA] * \frac{1}{t} \quad (1)$$

where *MG-MMA* is the rate of methanogenesis from MMA (nmol cm^{-3} d^{-1}); a_{CH4} is the radioactive methane produced from methanogenesis (CPM); a_{TIC} is the ^{14}C-TIC produced from the oxidation of methane (CPM); a_{MMA} the residual ^{14}C-MMA (CPM); RF is the recovery factor; *[MMA]* is the assumed MMA porewater concentrations (nmol cm^{-3}); *t* is the incubation time (d). $^{14}C\text{-}CH_4$ and ^{14}C-TIC sample activity was corrected by respective abiotic activity determined in dead controls.

Results from the ^{14}C-MMA incubations were also used to estimate the AOM-MMA rates according to Eq. (2),

$$AOM\text{-}MMA = \frac{a_{TIC}}{a_{CH_4} + a_{TIC}} * [CH_4] * \frac{1}{t} \quad (2)$$

where *AOM-MMA* is the AOM rate based on methane produced from MMA (nmol cm^{-3}d^{-1}); a_{TIC} is the produced ^{14}C-TIC (CPM); a_{CH4} is the residual radioactive methane (CPM); *[CH_4]* is the sediment methane concentration (nmol cm^{-3}); *t* is the incubation time (d). ^{14}C-TIC activity was corrected by abiotic activity determined by replicate dead controls.

2.7. AOM from ^{14}C-methane

AOM rates from $^{14}C\text{-}CH_4$ (AOM-CH_4) were determined by injecting $^{14}C\text{-}CH_4$ (dissolved in anoxic MilliQ, injection volume 10 μL, activity 5 KBq, Specific activity 1.85 − 2.22 GBq mmol^{-1}) directly into a separate small whole round core from each station at 1-cm intervals, similar to sections 2.5 and 2.6. Incubations were stopped after ~ 24 h and stored at room temperature until further processing, similar to section 2.6. Sediments were then analyzed in the laboratory using oven combustion (Treude et al., 2005) and acidification/shaking (Joye et al., 2004). The radioactivity captured was determined by liquid scintillation counting. AOM-CH_4 rates were calculated according to Eq. (2).

2.8. Metabolic rate constants for MG-MMA, AOM-MMA and AOM-CH_4

Experimental data determined by sect. 2.6 and 2.7 were used to calculate metabolic rate constants (k) to compare relative turnover of MMA and CH_4. We define the rate constants as the metabolic products divided by the sum of the metabolic reactants and products, divided by the incubation time (Krause et al., 2023).

2.9. Molecular analysis

2.9.1. DNA extraction from sediment

DNA was extracted from approximately 25–30 mg of sediment collected from all sediment intervals in the top ~ 20 cm of the solid phase push cores from all stations (see above section 2.2) using the PowerSoil DNA Extraction Kit (Qiagen) according to the manufacturer's instructions with the following modifications. Bead tubes were beadbeated for 45 sec at 5.5 m/sec. Samples were eluted first with 50 μL of elution buffer (Solution C6) followed by and additional 25 μl of elution buffer for a total of 75uL elution volume.

2.9.2. 16S rRNA gene sequencing (Illumina MiSeq)

The V4-V5 region of the 16S rRNA gene was amplified using archaeal/bacterial primers with Illumina (San Diego, CA, USA) adapters on 5′ end (515F 5′-TCGTCGGCAGCGTCAGATGTGTATAAGAGACAG-GTGYCAGCMGCCGCGGTAA-3′and 926R 5′-GTCTCGTGGGCTCGGA-GATGTGTATAAGAGACAG-CCGYCAATTYMTTTRAGTTT-3′). PCR reaction mix was set up in duplicate for each sample with Q5 Hot Start High-Fidelity 2x Master Mix (New England Biolabs, Ipswich, MA, USA) in a 15 μL reaction volume according to manufacturer's directions with annealing conditions of 54°C for 30 cycles. Duplicate PCR samples were then pooled and barcoded with Illumina Nextera XT index 2 primers that include unique 8-bp barcodes (P5 5′-AATGATACGGCGACCACCGA-GATCTACAC-XXXXXXXX-TCGTCGGCAGCGTC-3′ and P7 5′-CAAGCA-GAAGACGGCATACGAGAT-XXXXXXXX-GTCTCGTGGGCTCGG-3′). Amplification with barcoded primers used Q5 Hot Start PCR mixture but used 2.5 μL of product in 25 μL of total reaction volume, annealed at 66°C, and cycled only 10 times. Products were purified using Millipore-Sigma (St. Louis, MO, USA) MultiScreen Plate MSNU03010 with vacuum manifold and quantified using ThermoFisher Scientific (Waltham, MA, USA) QuantIT PicoGreen dsDNA Assay Kit P11496 on the BioRad CFX96 Touch Real-Time PCR Detection System. Barcoded samples were combined in equimolar amounts into single tube and purified with Qiagen PCR Purification Kit 28,104 before submission to Laragen (Culver City, CA) for 250 bp paired end sequencing on Illumina's MiSeq platform the addition of 15–20% PhiX.

2.9.3. Analysis of microbial community distribution and 16S rRNA gene sequence data

Sequence data was processed in DADA2 version 1.18 (Callahan et al., 2016). Adapters were removed using cutadept (Martin, 2011). Raw sequences were trimmed to 260 bp for forward reads, and 180 bp for reverse reads based on quality of reads. Reads shorter than 260/180 were removed. Error rate was calculated using DADA2's algorithm. Reads were denoised and merged into Amplicon Sequencing Variants (ASV), requiring a 12 bp overlap, and chimeras removed. Taxonomic identification for each representative sequence was assigned with the Silva-138 database (Quast et al., 2012) at 100% identity. The SILVA database had been appended with 1,197 in-house high-quality, methane seep-derived bacterial and archaeal clones. The modified SILVA database is available at NCBI BioProject PRJNA1199032.

To visualize the differences between each horizon at each station, a non-metric multidimensional scaling (NMDS) plot was generated. We used Bray-Curtis dissimilarity matrix to calculate the beta diversity of each sample. Each sediment horizon was plotted as an individual dot. The effect of various measured sediment geochemical parameters and calculated metabolic rate measurements for each horizon was calculated with the envfit function (vegan package, permutations = 999, (Oksanen et al., 2022) and plotted as arrows. The arrow vector length corresponds to the significance of its correlation with the NMDS. The length of the arrow corresponds to the significance (all $p < 0.05$).

3. Results

3.1. Geochemical trends across the salinity transect

3.1.1. Total organic carbon and nitrogen

The total organic carbon (TOC) and total organic nitrogen (TON) in the sediment varied across stations, generally decreasing with depth, except at the M station, where TOC increased with depth (Fig. 2 B, H, N, and T). The HP station had the highest surface TOC (5.4 wt%); however, values dropped sharply below 1.5 cm. TON trends generally followed the shape of the TOC profiles displaying the highest value (0.38 wt%) in the surface sediment of the HP station. The organic C/N ratio varied moderately with depth around 15 at the BL and BH stations, while slightly increasing with depth at the M station. At the HP station, C/N showed the highest values (28 and 25) with distinct peaks at 3.5–4.5 and 10.5–11.5 cm, respectively.

3.1.2. Total sulfide and iron (II) concentrations

At the BL and BH stations, porewater total sulfide concentrations were low (~6 μM; Fig. 2C and I) despite the high sulfate reduction activity (see section 3.2, Fig. 2D and J). At the M station, sulfide was higher than at the BL and BH stations (up to 86 μM), showing distinct peaks at the surface, in the middle of the core and at 15 cm (Fig. 2O), which coincide with sulfate reduction activity (Fig. 2P). At the HP station, sulfide exhibited multiple peaks located at the surface, mid-core, and at the bottom of the core (Fig. 2U), which also aligned with peaks of sulfate reduction activity (Fig. 2V). Iron (II) concentrations at the BL, BH and M stations increased with depth below the surface reaching 1219 μM, 1116 μM, and 1660 μM, respectively (Fig. 2C, I, and O). At the HP station iron (II) concentrations were consistently low (< 17 μM) throughout the sediment (Fig. 2U).

3.1.3. Salinity and sulfate concentrations

Refractometer measurements of the overlying surface water made in the field during low tide showed a natural salinity gradient with brackish conditions in the northern portion and more saline/hypersaline in the southern portions of the CSMR (Fig. 1). However, at the BL and BH stations, salinity and sulfate increased with sediment depth, reaching hypersaline (62 mM sulfate, 73 PSU at the BL station; 39 mM sulfate, 47 PSU at the BH station) conditions at the bottom of the core (Fig. 2D and J). At the M station, both parameters slightly decreased with increasing depth despite its proximity to the ocean (Fig. 2P). The HP station had the highest surface salinity (139 PSU) and porewater sulfate concentration (91 mM) (Fig. 2V). Both parameters decreased considerably with increasing sediment depth at the HP station.

3.1.4. Sediment methane concentrations

At the BL and HP stations, methane concentrations were consistently low (~10–15 μM) without a clear trend (Fig. 2F and X). The BH station had slightly elevated methane concentrations near the sediment surface (Max 28 μM) but fluctuated at lower concentrations below 4.5 cm (Fig. 2L). At the M station, methane was low (7 to 16 μM) in the top 6.5 cm, below which concentrations increased sharply with depth, exhibiting the highest concentrations (~665 μM) across the transect (Fig. 2R).

3.1.5. Substrates available for methanogenesis

Carbon substrates for methanogenesis (mono-methylamine, methanol, and acetate) in the porewater determined by NMR were mostly below the analytical detection limits (3 μM). Mono-methylamine was only found in surface sediments at the BL and HP stations and was below the quantification limit (10 μM). Methanol appeared in below quantification concentrations within the 9.5–10.5 cm intervals at the BL and BH stations and the 14.5–15.5 cm intervals at the M and HP stations but was undetectable in shallower sediment (0–1.5 cm) at all stations. Acetate was present in quantifiable amounts at specific depths BL (9.5–10.5 cm), BH (0–1.5 cm), and M (14.5–15.5 cm) reaching 61, 45,

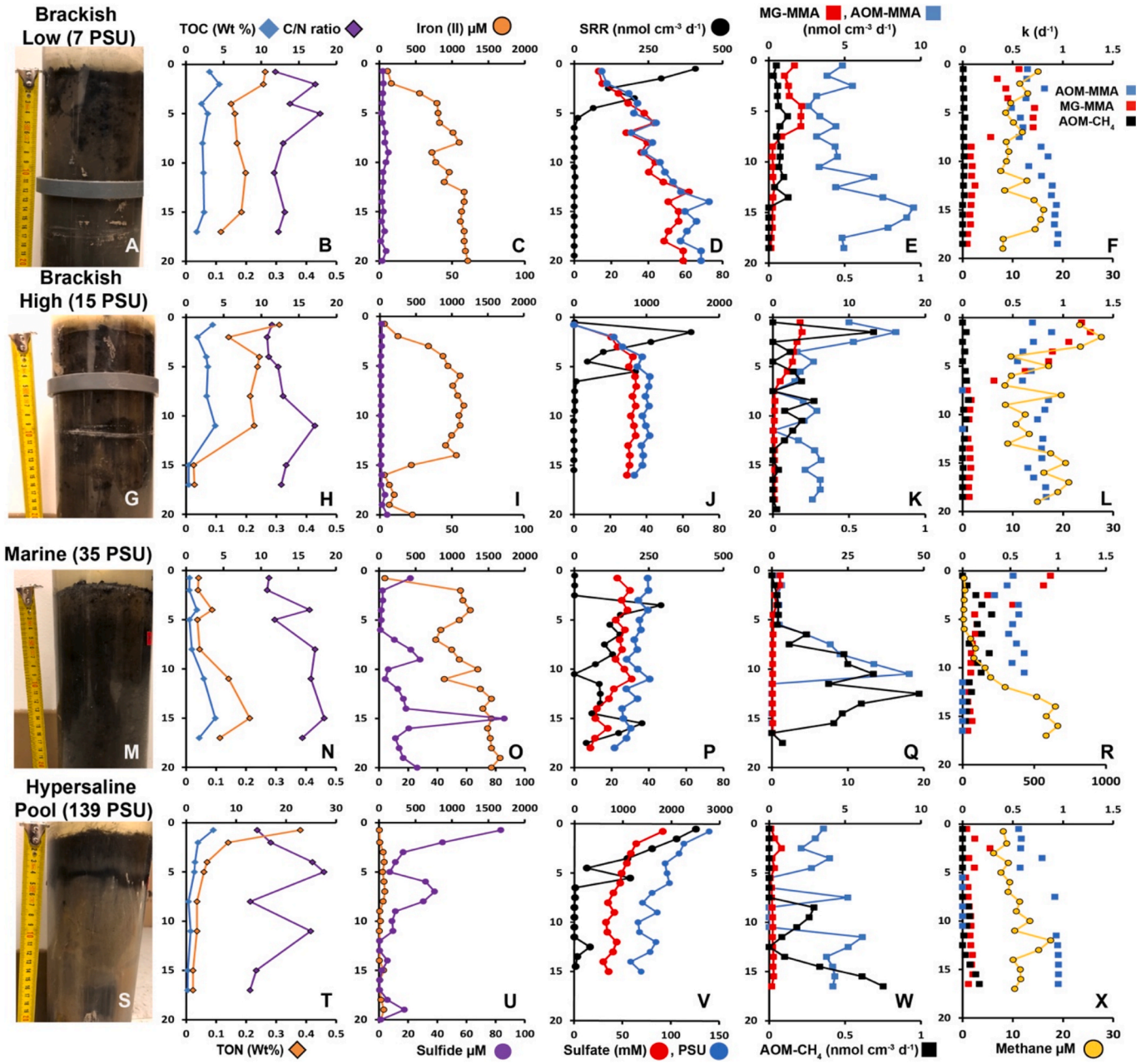

Fig. 2. Depth profiles of (bio)geochemical parameters determined in sediment cores collected from the four different stations in the Carpinteria Salt Marsh Reserve. Left Panel: Photos of the sediment cores collected (with scale) from the Brackish Low (A), Brackish High (G), Marine (M), and Hypersaline (S) stations. B, H, N, and T: TOC, TON and C/N ratio. C, I, O, and U: Porewater sulfide and iron (II). D, J, P, and V: ex-situ sulfate reduction rates (SRR), porewater sulfate, and porewater salinity. E, K, Q, and W: AOM rates derived from ^{14}C-mono-methylamine (AOM-MMA) incubations, methanogenesis rates from ^{14}C-mono-methylamine (MG-MMA) incubations, and AOM directly derived from ^{14}C-methane (AOM-CH_4) incubations. F, L, R, and X: Metabolic rate constants (k) of AOM-MMA, MG-MMA, AOM-CH_4 incubations and sediment methane concentration. Note scale changes on the x-axis.

72 µM, respectively, while acetate was below detection in all other samples.

3.2. *Sulfate reduction from ^{35}S-sulfate and AOM from ^{14}C-CH_4*

Sulfate reduction rates peaked directly at the surface at the BL station (409 nmol cm^{-3} d^{-1}; Fig. 2D), while AOM-CH_4 rates were constantly low (<0.12 nmol cm^{-3} d^{-1}; Fig. 2E). At the BH station, sulfate reduction rates were highest directly beneath the surface (1615 nmol cm^{-3} d^{-1}; Fig. 2J), aligning with peaks of AOM-CH_4 which showed elevated levels (up to 0.66 nmol cm^{-3} d^{-1}; Fig. 2K) in the top 2/3 of the core at the BH station. At the M station, sulfate reduction also peaked below the surface (290 nmol cm^{-3} d^{-1}; Fig. 2P) where AOM-CH_4 was lowest (Fig. 2Q). Beneath, sulfate reduction remained mostly at elevated levels while AOM-CH_4 increased with depth, peaking at 12.5 cm (19 nmol cm^{-3} d^{-1}) and declined below. Beneath the peaks at the three stations, sulfate reduction rates decreased significantly, with some cases falling below the detection limit. At the HP station sulfate reduction peaked beneath the surface with the highest rates detected across the transect (2506 nmol cm^{-3} d^{-1}; Fig. 2V). However, no AOM-CH_4 activity was detected in the top 7.5 cm at the HP Station (Fig. 2W). Rather below 7.5 cm, AOM peaked between 8 and 12 cm, where sulfate reduction was either low or below detection, and then AOM-CH_4 steadily increased reaching 0.75 nmol cm^{-3} d^{-1} at the bottom of the core.

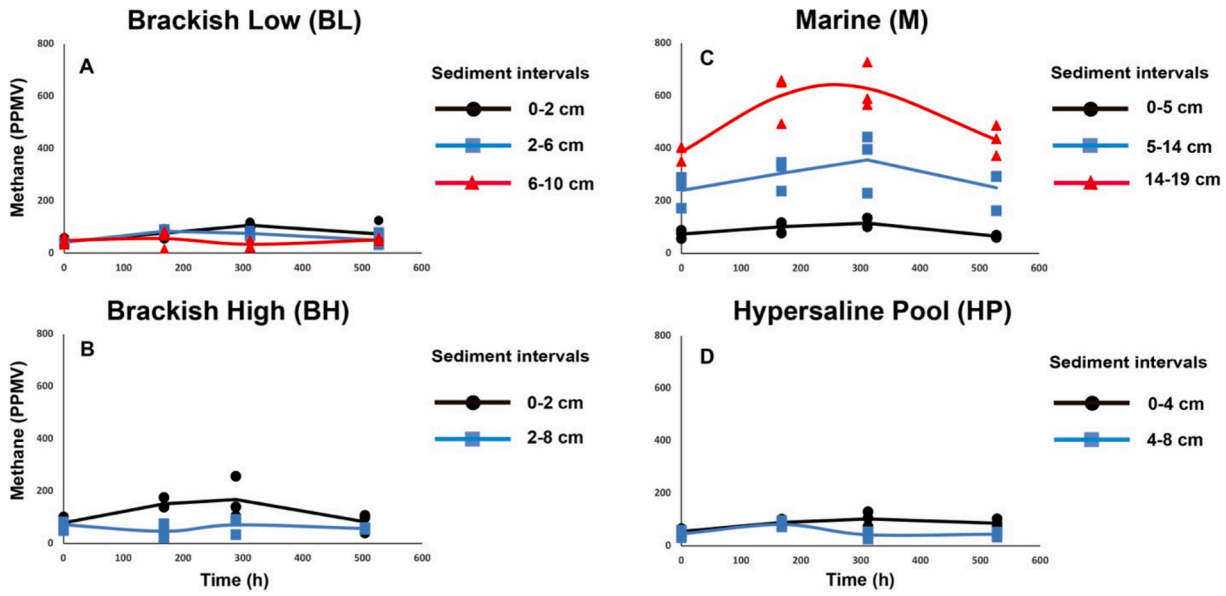

Fig. 3. Methane development during methanogenesis batch incubations with sediments from discrete sediment layers over time; (A) Brackish Low, (B) Brackish High, (C) Marine, and (D) Hypersaline Pool.

3.3. Methanogenesis and AOM from ^{14}C-MMA

3.3.1. ^{14}C-MMA recovery factor (RF)

RF values determined in sediment from BL, BH and M stations (see Sect. 2.6) were 0.66, 0.62, and 0.57, respectively, and were used to correct MG-MMA rates at each station.

3.3.2. MG-MMA and AOM-MMA

MG-MMA rates were highest near the sediment surface at all stations (Fig. 2E, K, Q, and W), aligning with the highest sulfate reduction activity (Fig. 2D, J, P, and V). The BH station had the highest rates (2 nmol cm^{-3} d^{-1}) out of all stations. In deeper sediment intervals (>5 cm) MG-MMA was consistently low (< 1 nmol cm^{-3} d^{-1}) but detectable at all stations (Fig. 2E, K, Q, and W).

AOM rates determined via ^{14}C mono-methylamine injections (AOM-MMA) rates were considerably higher than AOM rates determined by direct injection of ^{14}C-CH4 (AOM-CH$_4$) across all the stations (Fig. 2E, K, Q, and W). At the BL station, AOM-MMA fluctuated in the top 11 cm, then increased to reach a peak at 14–15 cm (10 nmol cm^{-3} d^{-1}). At the BH station, AOM-MMA had the highest rates in the top 3 cm (16 nmol cm^{-3} d^{-1}) and then fluctuated without trend in deeper intervals. At the M station, AOM-MMA rates increased below 6 cm similar to the AOM-CH$_4$ (Fig. 2Q), reaching a maximum (45 nmol cm^{-3} d^{-1}) at 10–11 cm. At the HP station, AOM-MMA rates highly fluctuated over the entire sediment core between active and non-active zones (Fig. 2W).

3.4. Metabolic rate constants

Metabolic rate constants (k) were plotted to allow for a more direct comparison between the turnover of different ^{14}C radiotracer species (Fig. 2F, L, R, and X). At the BL and BH stations, AOM-CH$_4$ had consistently low k values throughout the sediment cores, while MG-MMA k was highest near the surface and decreased with increasing sediment depth and AOM-MMA k remained high throughout. At the M station, k for AOM-CH4 was elevated between 2 and 11 cm and then declined. The MG-MMA k was high at the surface and then decreased with sediment depth, while the AOM-MMA k was high in the top 11 cm but reached zero, indicating no turnover, below. At the HP station, AOM-CH4 k was above zero only in specific depth ranges in the middle and bottom of the core. The MG-MMA k peaked at 2.5 cm but stayed otherwise low. The AOM-MMA k was high at most depth intervals with intermittent gaps where turnover was zero.

3.5. Methanogenesis batch incubations

Methane production remained low with only minor fluctuations at BL, BH, and HP stations (Fig. 3A, B, and D). At the M station, shallow sediments (0–5 cm) followed a similar pattern, but sediment from deeper intervals (5–14 cm and 14–19 cm) produced elevated methane levels, peaking in the middle of the incubation (312 h) (Fig. 3C).

3.6. Site dependent patterns in microbial community

Variation in the microbial community structure from 16S rRNA iTAG analysis (including bacteria and archaea) was observed between the 4 stations, (Fig. 4), with depth affiliated clustering of communities from the BL and BH stations relative to the M and HP stations. NMDS results showed that the communities within each horizon from the BL and BH grouped closer together, indicating similar beta diversity. Interestingly, microbial community structure at the M station showed two distinct groups, split by sediment depth. The microbial community structure at the HP station on the other hand, had the largest spread and was the least similar to the microbial communities from rest of the stations. To determine whether there were correlations between microbial community structure and corresponding geochemical and process rate data, laboratory incubation rates of matching cores as well as environmental factors were fitted onto the ordination using envfit command from the vegan R package (Oksanen et al., 2022). From this analysis, rates of MG-MMA were found to be significantly correlated (P-values = 0.014) with microbial communities in the BL and BH stations, while microbial community structure from station M was correlated with AOM-CH$_4$ and AOM-MMA rates (P-values = 0.001 and 0.007, respectively), and the HP community was correlated with sulfate reduction (P-value = 0.001).

Correlations were also observed between community structure and major geochemical parameters, including elevated salinity and sulfate at the HP site (P-value = 0.001), methane concentrations with the microbial community at station M (P-value = 0.001), iron (II) for BL and BH communities (P-value = 0.001), and sulfide for stations M and HP (P-value = 0.002).

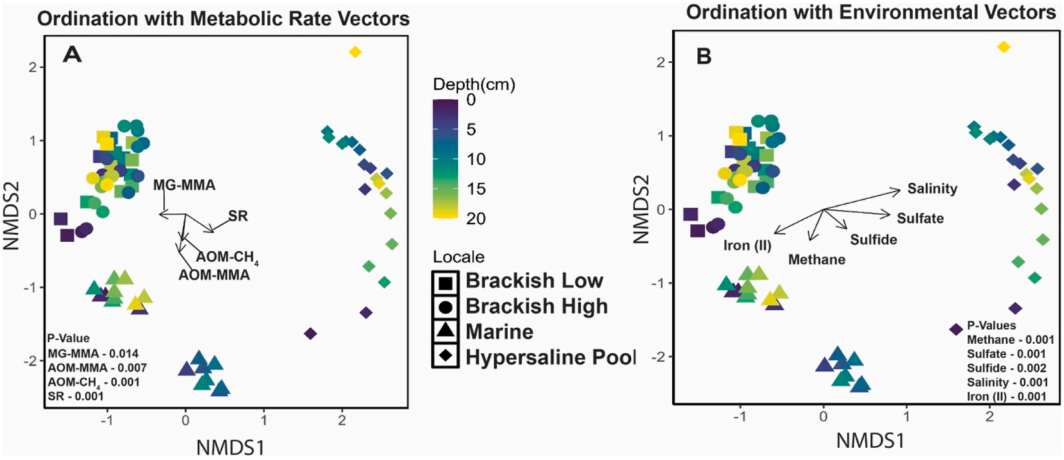

Fig. 4. NMDS plots showing microbial community structure of each station relative to each other, sediment depth, and correlations of microbial communities to metabolic rates (A) and geochemical parameters (B).

3.7. 16S rRNA iTAG analysis of microbial diversity

16S rRNA iTAG sequencing was used to characterize the archaeal (Fig. 5A-D) and bacterial (Fig. 5 E-H) diversity (above 1% relative abundances), with emphasis on methane related archaea and sulfate-reducing bacteria at each station within the CSMR transect (see sections 3.7.1 and 3.7.2). At the BL and BH stations, the most abundant archaeal amplicon sequence variants (ASVs) belonged to archaeal families of Bathyarchaeia (1–3.6% at BL; 1.1%–8.1% at BH), Lokiarchaeia (1.2%–4.8% at BL;1% at BH), Marine Benthic Group D and DHVEG-1 (1.4%–5.7% at BL; 1.2%–4% at BH), and uncultured families within Thermoplasmatota (0.05%–1.85% at BL; 0.06%–1.25% at BH) (Fig. 5A and B). At the M station archaeal ASV's increased with increasing sediment depth and mostly belonged to Woesearchaeales (1.2%–9.8%) and the SCDC AAA0110D5 family of the Nanoarchaeota phylum (1.3%–10.4%) (Fig. 5C). At the HP station archaeal ASVs were highest out of all stations belonging to a variety of families of Haloferacaceae reaching up to 33% in the upper half of the core. Below, lower relative abundances of Haloferacaceae (Haloferacaceae_1) (1.2%–9.4%) and Nitrosopumilaceae (1.2%–10.7%) ASVs were also detected.

Bacterial ASVs belonging to the Pseudomonadales (formerly Proteobacteria) were present throughout all sediment depths from all stations but more prevalent in the top half of the sediment core from the BL, BH, and M stations (26%–35%), and were abundant throughout the sediment at the HP station (5.5%–45%) (Fig. 5E, F, G, and H). At the BL and BH stations bacterial ASVs belonging to Planctomycetota are more prevalent in sediment intervals below 7 cm, reaching 29% and 24%, respectively (Fig. 5E and F). At the M station, ASVs belonging to Planctomycetota are present throughout the sediment (Fig. 5G) but are lower than at the BL and BH stations, reaching 12%.

3.7.1. Methanogenic and methanotrophic signals

A main goal of this study was to identify methanogenic and methanotrophic archaea that could potentially be contributing to methane cycling across the transect. The most abundant groups of methane related archaea (above 0.1% relative abundances) across the transect, included known methanogens (*Methanosarcinaceae*, *Methanosaetaceae, Methanoregulaceae, Methanomassiliicoccales*, Methanofastidiosales, and *Methanonatronarchaeacea*) and anaerobic methanotrophs (Candidatus orders Methanocomedens, Methanomarinus, and Methanogastraceae (ANME 2a-c));(Chadwick et al., 2022). The groups of methanogens listed above can be found in anoxic sediments within a wide range of environments such as marine environments, acidic peat bogs, anaerobic reactors, oil fields, rice paddy soil, a mud volcano, and in freshwater lakes, and hypersaline environments (Oren, 2014; Sorokin et al., 2018). These methanogens produce methane using substrates such as acetate (*Methanosarcinaceae* and *Methanosaetaceae*), methylated substrates (*Methanosarcinaceae*, *Methanomassiliicoccales*, and *Methanonatronarchaeacea*), and/or H_2/CO_2 (*Methanosarcinaceae*, *Methanoregulaceae*, *Methanomassiliicoccales*, and *Methanonatronarchaeacea*) (Liu and Whitman, 2008; Oren, 2014; Sorokin et al., 2018).

The Ca. Methanocomedens and Ca. Methanomarinus (ANME-2a and -2b, respectively) lineage are commonly found in diverse methane-rich deep-sea and coastal marine environments (Orphan et al., 2001a; Orphan et al., 2001b; Ruff et al., 2016) and salt marsh sediment, mud volcanoes, hydrothermal vents (ANME-2a), and frequently co-exist with members of the Methanogasteraceae (ANME-2c) in methane seeps (Knittel and Boetius, 2009; Knittel et al., 2018). ANME-2c has additionally been reported from a freshwater coastal aquifer (López-Archilla et al., 2007). All of these methanotrophic ANME-2 have been found to partner with diverse syntrophic sulfate-reducing bacteria to couple AOM with sulfate reduction (Knittel and Boetius, 2009; Knittel et al., 2018; Murali et al., 2023; Timmers et al., 2017).

The BL and BH stations had the lowest relative abundance of archaea putatively associated with methane metabolism (Fig. 6A and B), with overall relative abundances <2.5% from the families of Methanosarcinaceae and <1% relative abundance of uncultured *Methanomassiliicoccales*, and uncultured Methanofastidiosales. At the BH station ASVs affiliated with one group of anaerobic methanotrophic archaea (ANME-2c) was detected at 5.5–6.5 cm (0.15%). Otherwise, no other groups of ANME were detected in the brackish BL and BH stations, which is consistent with low AOM activity measured at these stations (Fig. 2E and K). At the M station, the relative abundance of ASV's affiliated with both methanogenic and methanotrophic archaea were more prevalent than at any of the other stations (Fig. 6C), here also corresponding with some of the highest AOM rate measurements (Fig. 2Q). Methanotrophic ANME-2a and b were dominant over methanogenic archaeal lineages, reaching 6.5% and 5.3% in distinct depths within the upper half of the core compared to 0.45% for *Methanosarcinaceae* and 2.3% for the uncultured *Methanomassiliicoccales* (Fig. 6C). ANME-2c ASVs were also detected at low relative abundance alongside ANME-2a and b reaching 0.48% and 0.73%. At 12.5–13.5 cm, ASVs belonging to methanogenic archaeal families of *Methanosarcinaceae*, *Methanosaetaceae*, *Methanomassiliicoccales*, and *Methanoregulaceae*, (0.41%, 0.85%, 0.65%, and 0.53%, respectively,) alongside with ANME 2a-2b and 2c archaeal ASVs (5.3% and 0.73%, respectively) at this depth interval (Fig. 6C). This coincides with estimated rates of MG-MMA (0.17 nmol cm^{-3} d^{-1}), the highest AOM-CH_4 (19 nmol cm^{-3} d^{-1}) (Fig. 2Q), and elevated methane concentrations (297 μM); (Fig. 2X). Below 13.5 cm, a higher percentage of the ASV

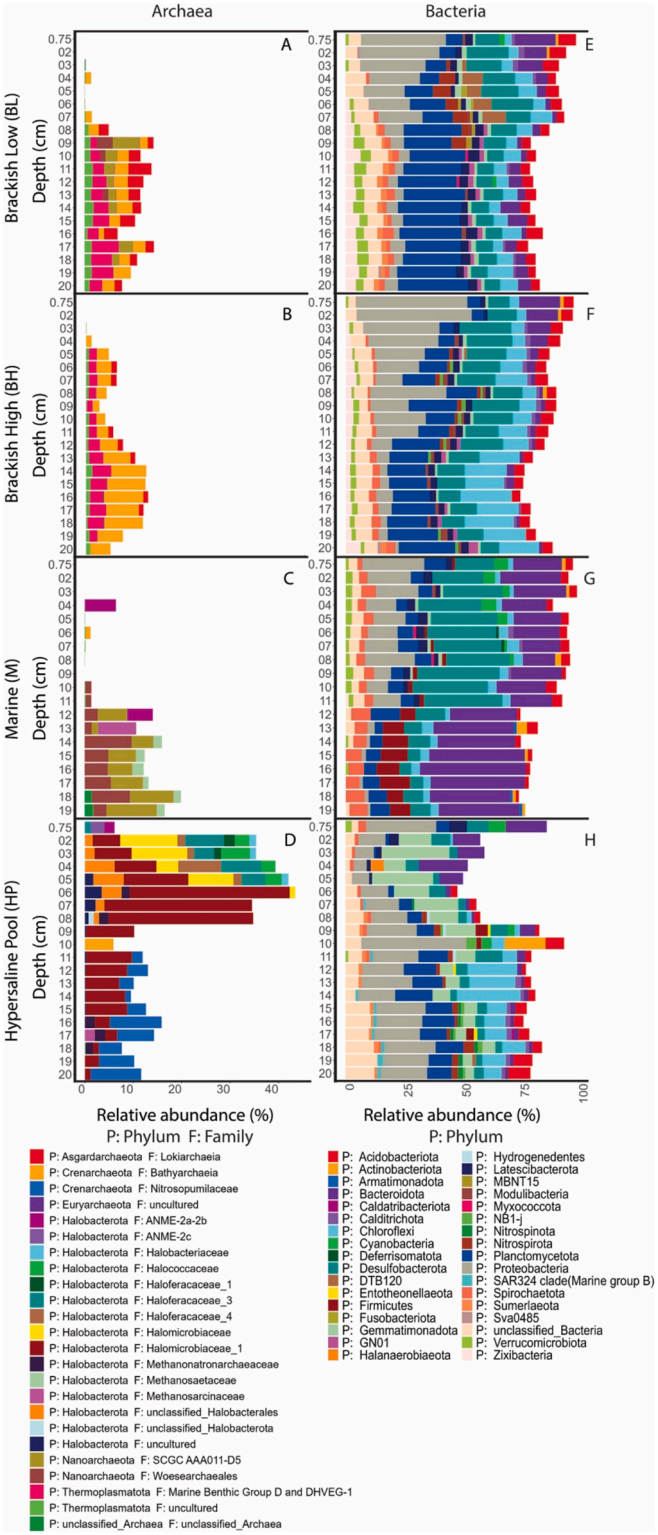

Fig. 5. 16S rRNA iTAG relative abundances of archaeal phyla above the 0.1% relative abundance threshold (A-D) and of the top 36 bacteria phyla (E-H) detected in the sediment of the CSMR transect. Note the differences in x-axis scale.

belonged to *Methanosarcinaceae*, *Methanosaetaceae*, *Methanomassiliicoccales*, *and Methanoregulaceae* reaching 7.8%, 2.3%, 0.74% and 0.95%, respectively (Fig. 6C).

At the HP station, ASVs belonging to ANME-2a, −2b, and –2c were detected in the top 2.5 cm, reaching 2.8% and 2.1%, respectively. This coincides with detectable AOM-MMA activity but not with AOM-CH_4 activity, which were below detection at these depth intervals (Fig. 2W). Below 2.5 cm, methanotrophic ASVs were not recovered (Fig. 6D), but AOM was detectable at low rates (Fig. 2W). Methanogenic ASVs belonging to the family *Methanonatronarchaeacea,* a methylotrophic methanogenic group previously described from hypersaline environments (Sorokin et al., 2018),were detected in deeper sediment intervals at 2.1%, where MG-MMA activity was also detected (Fig. 2W). *Methanosarcinaceae* ASV's were also recovered at the bottom of the core (Fig. 6D).

3.7.2. *Distribution of sulfate-reducing bacterial taxa*

Members within the Desulfobacterota phylum are the dominant sulfate-reducing organisms that are found in surface marine and freshwater sediments (Diao et al., 2023; Waite et al., 2020). Many members within this sulfate-reducing phylum (Geobacterales, Geopsychrobacteraceae, Geothermobacteraceae, Desulfuromondaceaae, Desulfobacterales, Desulfobulbales, and Desulfovibrionales) are also capable of iron reduction (Holmes et al., 2004; Park et al., 2008; Reyes et al., 2017; Waite et al., 2020; Young, 2003). Several known sulfate and iron-reducing bacterial groups were detected across the transect (Fig. 7A–D) which coincide with high sulfate reduction rates and porewater iron (II) concentrations (Fig. 2C, D, I, J, O, P, U, and V). At the BL and BH stations, Desulfobulbales and Desulfobacterales (part of Desulfobacterota 1) ASV trends were similar, however, the abundances of Desulfobacterales were higher and extended to the bottom of the core at the BH station. Thermodesulfovibrionia were detected in both the BL and BH stations. They were more abundant at the BL station within the top half of the core ranging 1.4%–11%, versus 0.5%–1.5% in the middle and bottom portions of the core at the BH station (Fig. 7A and B). The BL station was the only station containing Desulfuromonadaceae within a narrow sediment layer in the middle of the core reaching 3.4%. Syntrophobacterales were detected at both the BL and BH stations at low abundances (<2%). They were found in more sediment layers in the middle and towards the bottom of the core at the BH station. Stations BL and BH were the only stations containing Desulfatiglandales ranging between 1% and 4.5%, in the middle to lower half of the core. At the top of the core from the BH station, Desulfuromonadia were detected (~1.5%). At the M station, Desulfobacterales abundances were the highest in the top half of the core reaching 26.9% and then declined below 12 cm ranging between 1.3%–4.6% (Fig. 7C). Desulfobulbales were also detected in the top 11 cm ranging between 4.1%–7.4%. The M station was the only station containing ASV's belonging to Desulfuromonadia (ranging between 1.3% and 4.3%), Geobacterales (ranging between 1.4% and 4.7%), and Syntrophales (ranging between 1% and 1.4%) in the top 11.5 cm, below 12.5 cm, and below 16.5 cm, respectively. The HP station had the least amount of ASVs belonging to phyla capable of sulfate reduction (Fig. 7D), despite having the highest sulfate reduction activity out of all stations (Fig. 2V). Desulfobacterales and Desulfobulbales were detected in the top and middle portions of the core ranging between 1.1%–7% and 1%–2%, respectively. One sediment interval near the surface of the core had ASV's belonging to Desulfovibrionales at low relative abundance (2%); (Fig. 7D). The HP station was the only station containing ASV's belonging to Geothermobacteraceae in the middle and bottom of the core, ranging between 1% and 4.3%, where smaller concentrations of porewater iron (II) were detected (Fig. 2U). Thermodesulfovibrionia and Syntrophobacterales were also detected in the HP station in the middle and bottom of the core ranging 0.4%–4.5% and 1.2% −2.8%, respectively (Fig. 7D).

4. Discussion

4.1. *Spatial evidence of cryptic methane cycling*

The aim of this study was to find evidence of cryptic methane cycling across the land–ocean transect in the CSMR, by presenting geochemical

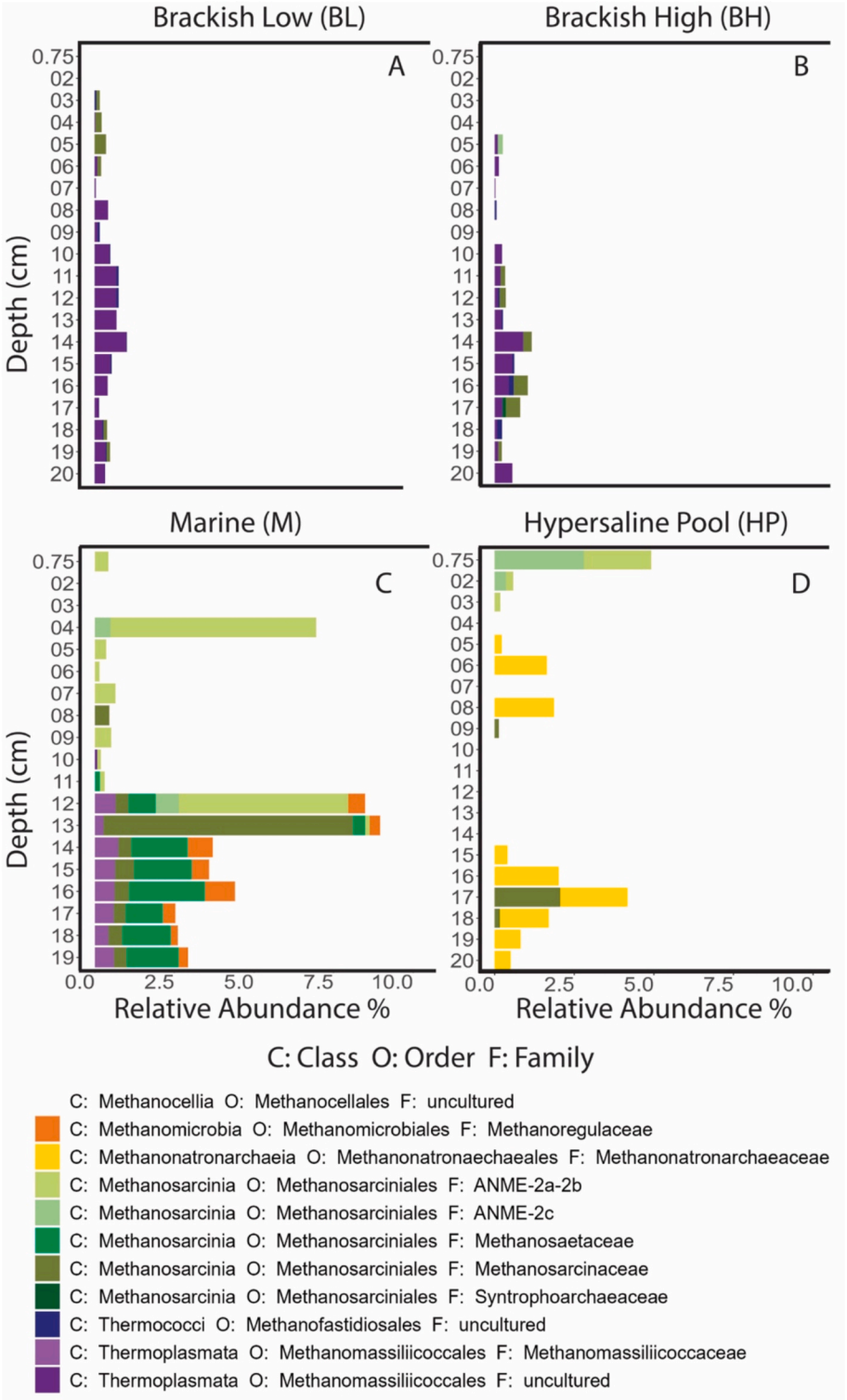

Fig. 6. Relative abundances of putative methanogenic and anaerobic methanotrophic archaea (A-D) along the CSMR transect.

evidence along with concurrent activity of methanogenesis from monomethylamine (in the following termed 'methylotrophic methanogenesis'), sulfate reduction, and AOM from radiotracer incubations (^{14}C-MMA, ^{35}S-SO_4^{-2}, and ^{14}C-CH_4, respectively). Based on the development of ^{14}C-methane in our ^{14}C-MMA incubations, methylotrophic methanogenesis appears to be active at all stations and throughout the sampled intervals. Radiotracer experiments further suggested that methylotrophic methanogenesis overlapped with sulfate reduction and AOM in the 0–14, 1–19, 1–18, and 7–17 cm sections at the BL, BH, M, and HP stations, respectively (Fig. 2D, E, J, K, P, Q, V, and W).

Methylotrophic methanogenesis rates at all depth intervals and stations reported in this study were calculated assuming a porewater monomethylamine concentration of 3 μM which is the detection limit of the NMR analysis (see sections 2.4 and 2.6). Mono-methylamine tends to bind to mineral surfaces within sediments (Wang and Lee, 1993, 1994; Xiao et al., 2022), which was observed along the CSMR transect based on

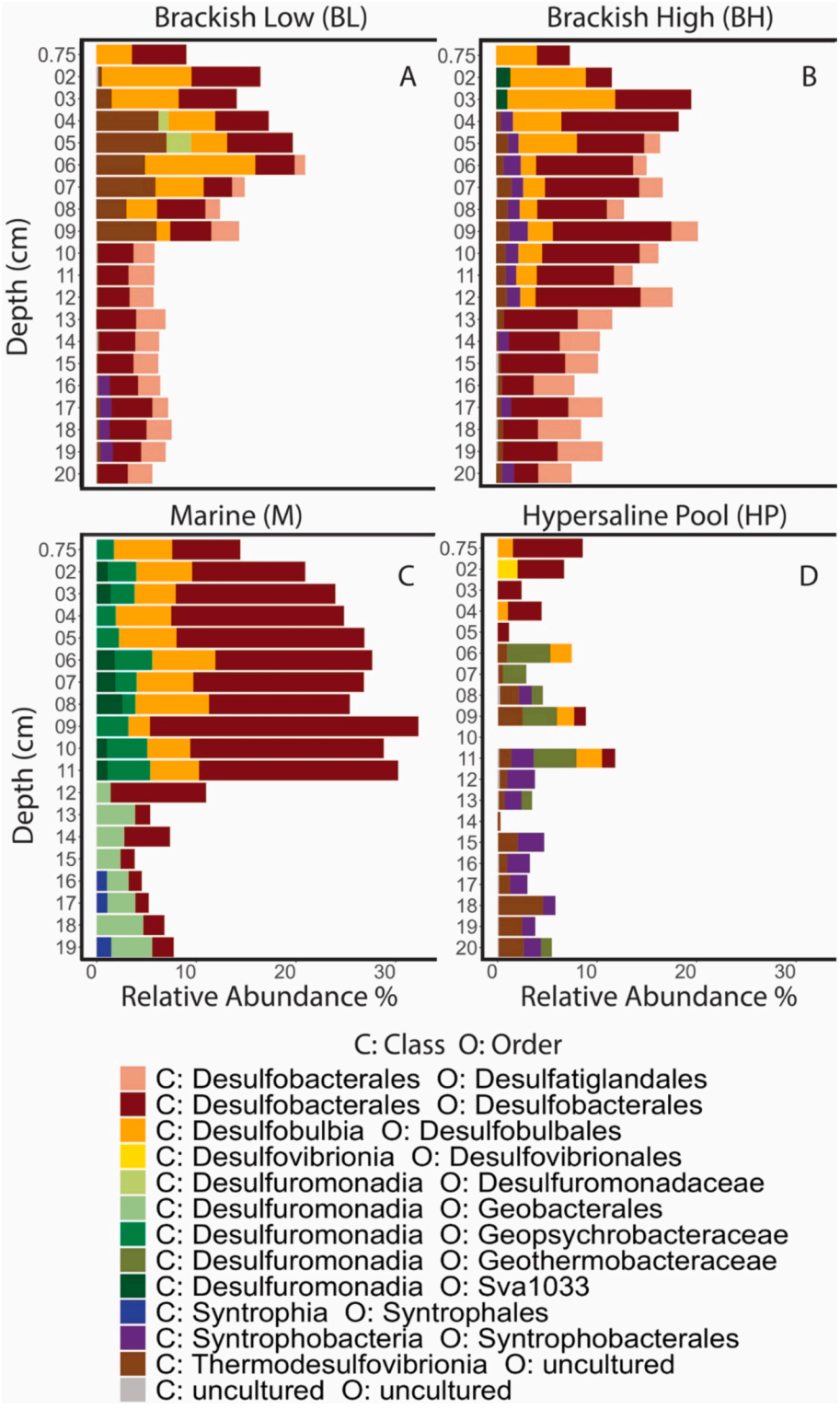

Fig. 7. Relative abundances of bacterial classes and orders within the Desulfobacterota phylum (A-D) along the CSMR transect.

the RF reported in section 3.3.1 and in Krause and Treude (2021). However, a recent study suggested that methylamines adsorbed to mineral surfaces may not be bioavailable to methylotrophic methanogenesis and thus cryptic methane cycling (Xiao et al., 2022). Since all porewater mono-methylamine concentrations were either below detection or below quantification (see section 3.1.5), assuming 3 μM monomethylamine in our rate calculations allows for the most conservative estimates of methylotrophic methanogenesis rates possible.

Our data suggest that the activity of sulfate reduction and methylotrophic methanogenesis is driven by the availability of organic matter. For example, higher TOC and TON were found within the top 2.5 cm at both the BL and BH stations (Fig. 2B and H) coinciding with the detection of the highest rates of sulfate reduction and methylotrophic methanogenesis (Fig. 2D, J, E, and K). Halotolerant grasses and algae were found on the embankments and submerged within streams at the BL and BH stations (Fig. 1), likely supplying some of the organic matter

detected, which has been shown to enhance sulfate reduction (Jackson et al., 2014; Kostka et al., 2002) and methanogenesis (Yuan et al., 2014; Yuan et al., 2019) in coastal salt marsh sediments. Conversely, at the M station lower TOC and TON content was detected (Fig. 2N), potentially explaining lower or undetectable sulfate reduction and methylotrophic methanogenesis activity within the top 10 cm (Fig. 2P and Q). Field and lab observations of the sediment from the M station indicated a larger sediment grain size (sand) in the top 10 cm. Previous work has shown that permeable sands are sites of enhanced organic matter turnover (Boudreau et al., 2001) because flow into permeable sandy sediment delivers more particulate organic material (Huettel et al., 1996; Rusch et al., 2001) and oxygen (Booij et al., 1991; Precht et al., 2004; Ziebis et al., 1996), and quickly removes products of degradation (Huettel et al., 1998; Rocha, 1998). This flushing process from daily tidal influence likely prevents sediment near the surface from becoming fully anoxic, inhibiting sulfate reduction and methanogenesis in surface sediment of the M station.

Different to Krause and Treude (2021), who found concurrent peaks of methylotrophic methanogenesis and AOM in the top 5 cm at the HP station, overlap of the two processes was detected only in deeper sediment intervals (>12 cm, Fig. 2W) in the present study. Here sediment from the HP pool was collected approximately one year after and one meter away from the original sampling spot studied in Krause and Treude (2021), suggesting that cryptic methane cycling activity is subject to natural temporal and spatial variation at this site. Coastal wetlands, including salt marshes, are highly dynamic ecosystems that exhibit spatial heterogeneity in the sediment redox potential (Cui et al., 2024). This variability complicates efforts to accurately quantify the methane contribution of coastal wetlands to the global methane budget (Rosentreter et al., 2023; Saunois et al., 2025). Therefore, the significant differences in the rates observed in the present study compared to those of Krause and Treude (2021) may be attributed to spatial and temporal variability.

Based on the ^{14}C-methane produced during the ^{14}C-MMA incubations (Fig. 2E, K, Q, W) methane detected within sulfate-rich sediment is likely sourced from methylotrophic methanogenesis. Methane in the sediment from the BL, BH, and HP stations were about an order of magnitude lower (Fig. 2F, L, and X) than what has been previously reported from the top 20 cm of sediment at other coastal wetlands, such as the Arne Peninsular salt marsh, UK (up to 100 μM) (Parkes et al., 2012), the Queen's Creek Tidal Marsh, VA, USA (up to 450 μM, in July) (Bartlett et al., 1987), the Chongming Island of the Yangtze Estuary, East Asia (up to 156 μM) (Li et al., 2021), and Dover Bluff salt marsh, GA, USA (0.3–1.2 mM) (Segarra et al., 2013). Present but low methane could represent the equilibrium between methylotrophic methanogenesis and AOM as part of the cryptic methane cycle in sulfate-reducing sediment (Krause et al., 2023). The observed methane profiles at these three stations are opposite the classical diffusion-controlled trend where residual methane linearly declines between the SMTZ and the sediment–water interface, which is often seen in salt marshes, tidal marshes and estuaries (Bartlett et al., 1987; Parkes et al., 2012; Segarra et al., 2013) and marine environments (Bernard, 1979; Iversen and Jørgensen, 1993; Lapham et al., 2024; Reeburgh, 2007; Tilbrook and Karl, 1995). Methane profiles at the BL, BH, M (top 5 cm), and HP stations were more similar to organic-rich surface sediment in the oxygen-deficient Santa Barbara Basin, where the simultaneous production and consumption of methane was also detected (Krause et al., 2023). In contrast to the three stations, the methane profile at the M station showed a typical increase with depth, likely approaching the shallow end of the SMTZ, similar to patterns observed in other marine sediments (Bernard, 1979; Lapham et al., 2024; Reeburgh, 2007; Tilbrook and Karl, 1995). Given that the sulfate concentration was still ~ 9 mM at the bottom of the core, the actual transition zone is expected to be located much deeper.

Additional support for the presence of cryptic methane cycling in the salt marsh sediments comes from the methanogenesis batch incubations (Fig. 3A, B, C and D), which show no linear buildup of methane in the headspace over ~ 530 h, except in sediment from deeper layers (>5cm) of the M station. While there are two ways to interpret the lack of methane build up in the batch incubations, i.e., either the absence of methane production or the presence of simultaneous methane production and consumption, our radiotracer data point towards the latter scenario. Together, the radiotracer and batch incubations strongly suggest simultaneous methane production and consumption by the cryptic methane cycle across the transect.

4.2. Spatial geochemical trends and electron acceptors for AOM

Another goal of this study was to compare porewater salinity and electron acceptor availability with metabolic processes (i.e., sulfate reduction and AOM) along the transect. Although the salinity in the overlying water indicated a natural salinity gradient across the CSMR due to freshwater and seawater convergence, the porewater salinity and sulfate concentrations in the two brackish stations unexpectedly increased with increasing sediment depth (Fig. 2D and J). This finding suggests that the sediment hydrology of the CSMR is not in steady state, but is instead strongly influenced by seawater infiltration, rather than by freshwater inputs from more inland watersheds. The abundance of salt within salt marshes such as the CSMR is largely controlled by tidal infiltration and inundation and by evaporation (Gardner, 2007; Li et al., 2023; Moffett et al., 2010). It is conceivable that subsurface hydrology and the geomorphology of the CSMR plays a role in the salinization and/or dilution of the salt in the subsurface of the CSMR (Reddy et al., 2022). However, the present study did not determine the direction of seawater penetration/infiltration (vertical or lateral diffusion) but future studies at the CSMR and other coastal wetlands would benefit from such determinations because the seawater delivers sulfate, which is a key electron acceptor for AOM.

Across the CSMR transect, porewater sulfate was mostly high (≥9 mM) supporting high sulfate reduction activity in the top 5–10 cm (Fig. 2D, J, P, V). Sulfate further strongly correlated with microbial communities at the HP station (Fig. 4A), which had the highest sulfate reduction rates (Fig. 2V). While sulfate reduction was likely linked to organic matter degradation, it also could be coupled to AOM in layers where both processes coincided (Fig. 2D, E, J, K, P, Q, V, and W). In support of this hypothesis, 16S sequencing data confirmed the presence of bacterial groups capable of sulfate reduction (Fig. 7C and D) in all layers where ANME groups were found (Fig. 6C and D) and where sulfate reduction and AOM activity overlapped (Fig. 2D, J, P, and V), except at the BL and BH stations, where ANME groups were not detected (see section 4.3 for details).

Across the lateral transect, the porewater profiles of iron (II) and sulfide (Fig. 2C, I, O, and U) showed that sediment below the top 2 cm transitioned from an iron-reducing environment (higher Fe (II), absence of sulfide) at the BL station, to a simultaneous iron and sulfate-reducing environment (both Fe (II) and sulfide present) at the M station, and finally to a sulfate-reducing environment (low Fe (II), higher sulfide presence) at the HP station. The microbial community analysis shows a strong correlation between high iron (II) and microbial communities at the BL, BH, and M stations suggesting the presence of groups that are involved in iron cycling (Fig. 4B). Furthermore, 16S rRNA sequencing recovered members of the Acidobacteriota, Firmicutes, Deferrisomatota, and Sva 0485 phyla, which are bacterial phyla and orders known to contain lineages of iron-reducing bacteria (Holmes et al., 2004; Park et al., 2008; Reyes et al., 2017; Waite et al., 2020; Weber et al., 2006) which may be contributing to the buildup of iron (II) at these stations (Fig. 5E, F, and G and Fig. 7A, B, and C).

The sulfide production at the M and HP stations is likely attributed to the widespread sulfate reduction activity at both stations, which can be either coupled to organic matter degradation or AOM (Fig. 2O, U, P and V). These findings fit with the microbial community data (Fig. 4A and B), which show that microbial communities at the M station are correlated with sulfide and AOM, pointing to sulfate-dependent AOM, while

at the HP station communities are correlated with sulfide concentrations and sulfate reduction activity, pointing to organoclastic sulfate reduction. The 16S rRNA gene diversity at the M and HP stations shows the presence of sulfate/iron-reducing bacteria throughout the sediment (Fig. 7C and D) which could potentially be contributing to sulfate reduction activity and buildup of both sulfide and iron (II) in the sediment at the M station (Fig. 2O and P) as well as, the high sulfate reduction activity and buildup of sulfide at the HP station (Fig. 2U and V).

The geochemical and molecular data in this study strongly indicate that both iron and sulfate reduction are concurrently active at all stations (Fig. 2C, I, O, and U, Fig. 2D, J, P, and V and Fig. 7A–D). Similar overlaps between sulfate reduction activity and porewater iron (II) profiles–indicating concurrent iron and sulfate reduction–have been observed in marine (Postma and Jakobsen, 1996), lacustrine (Motelica-Heino et al., 2003), tropical mangrove (Holmer et al., 1994), and salt marsh (Gribsholt and Kristensen, 2002; Hyun et al., 2007; Koretsky et al., 2003; Lin et al., 2020; Reddy and DeLaune, 2008) sediment environments. The observation of simultaneous iron and sulfate reduction activity is interesting since iron reduction is thermodynamically more favorable than sulfate reduction for shared substrates such as hydrogen and acetate (Jørgensen, 2000) and would typically suppress sulfate reduction activity (Lovley and Phillips, 1987). This may be linked to the presence of iron oxides that are more crystalline in structure which have been shown to shift microbial communities to favor sulfate reduction over iron reduction even in iron-rich sediment creating inverse redox zonation (Hansel et al., 2015; Lentini et al., 2012). Alternatively, iron oxides have been shown to persist even below sulfate reduction layers in sedimentary environments that receive high inputs of iron-oxides and/or have sediments that have undergone transient diagenesis (Egger et al., 2015). This is true at the HP station where Liu et al., (2025) showed that microbial iron reduction is in competition with aqueous sulfide, produced from sulfate reduction, for poorly-crystalline iron oxides. This diagenetic alteration leads to the formation of iron sulfides and lower availability of poorly-crystalline iron oxides for microbes allowing for sulfate reduction to dominate in shallower sediment layers and pushing iron-reduction to deeper layers. The present study did not determine the quantity nor the types of iron oxides that may be in the sediment along the rest of the CSMR transect (i.e., BL, BH and M stations). Future investigations at the CSMR should direct attention to the dynamics between iron and sulfur systems in the brackish and marine portions of the CMSR as both iron (III) and sulfate are important electron acceptors for AOM in the cryptic methane cycle (see details below).

At the M station, ANME 2-a and -c (Fig. 6C), which have recently been demonstrated to be capable of iron-dependent AOM in marine sediments (Aromokeye et al., 2020; Scheller et al., 2016), were found. Although this study did not directly test for the coupling of iron to AOM, our study shows a substantial buildup of iron (II) in the sediment at BL, BH and M stations (Fig. 2C, I, and O) and a slight buildup of iron (II) in the presence of sulfide at the HP station (Fig. 2U) indicating that iron (III) could potentially be an important electron acceptor for AOM. Recent work at the CSMR does strongly suggest that both sulfate and iron (III) are important electron acceptors for AOM linked to cryptic methane cycling at the HP station (Liu et al., 2025). The decoupling of sulfate reduction and AOM rates in this study supports iron-dependent AOM as the dominant pathway of AOM in the surface sediment of the HP station (Fig. 2V, W). Although dissolved iron (II) concentrations in the HP station are considerably lower than at the other three stations, the dissolved iron (II) concentration at the HP station in 2019 (this study) was one to two orders of magnitude lower than in 2021 (Liu et al., 2025). The balance between porewater iron (II) and sulfide concentrations is likely attributed to seasonal changes in salinity. Salinity influences the activity of sulfate reduction at the HP station, as noted in the Krause and Treude (2021) study. The extent of sulfate reduction activity modulates the geochemical iron-sulfur conditions, ranging from high-Fe^{2+}/low-H_2S to low-Fe^{2+}/high-H_2S, because sulfide production from microbial sulfate reduction "titrates" porewater iron (II) abiotically (Poulton et al., 2004; Raiswell and Berner, 1985). Intense sulfate reduction in surface sediments enhances the downward flux of aqueous sulfide into the iron reduction zone, reducing the porewater iron (II) concentration. Therefore, relying on porewater geochemistry alone may obscure active microbial iron reduction, which is at least partially coupled to AOM linked to cryptic methane cycling.

In summary, our study shows that CSMR sediments are rich in sulfate and iron (Fig. 2C, D, I, J, O, P, U, and V), supporting organoclastic sulfate- and iron-reducing communities (Fig. 7). These sediments thereby not only regulate methane emissions by suppressing competitive methanogenesis but also support AOM, as part of the cryptic methane cycle, linked to potentially both sulfate and iron reduction (Fig. 2E, K, Q, W). Iron-dependent AOM has been shown to occur in marine (Beal et al., 2009; Rooze et al., 2016; Schnakenberg et al., 2021), brackish (Egger et al., 2017; Egger et al., 2015), freshwater (Bar-Or et al., 2017; Ettwig et al., 2016; Leu et al., 2020; Martinez-Cruz et al., 2018), and coastal wetland environments (Liu et al., 2025; Segarra et al., 2013; Valenzuela et al., 2019; Wallenius et al., 2021). Iron (III) could be an important electron acceptor for AOM in the sampled surface sediments at all stations, where dissolved iron (II) is present (Fig. 2). However, ANME lineages that are known to conduct iron-dependent AOM were only detected at the M and HP stations (Fig. 6C and D).

4.3. Archaeal methanogen and methanotroph communities

Another goal of this study was to elucidate the potential archaea lineages responsible for methanogenesis and AOM activity across the CSMR transect and to investigate whether they cooccur in the same sediment horizons, consistent with the potential for cryptic methane cycling in the CSMR. At the BL and BH stations, methylotrophic methanogenesis activity was strongly correlated with microbial community composition (Fig. 4A). At the BL and BH stations, low abundances of *Methanosarcinaceae* (Fig. 6A and B), a methanogenic family capable of producing methane from methylated substrates (Boone et al., 2015), overlapped with methylotrophic methanogenesis (Fig. 2E and K). Bathyarchaeia, detected at the BL and BH stations, may also contribute to the methylotrophic methanogenesis activity observed there. Metabolism reconstructions from metagenomes revealed that some groups of Bathyarchaeia have genes encoding for the methyl-coenzyme M reductase complex and are potentially capable of both methylotrophic methanogenesis and methane-oxidation (Evans et al., 2015; Hou et al., 2023). However, this archaeal group is highly diverse, and the evidence presented in this study does not directly link the methanogenesis activity to Bathyarchaeia. Future studies should investigate the potential contribution of these groups to the global methane budget.

At the M station, the relative abundance of ANME 2a-c dominated over methanogen lineages in shallower sediment intervals (Fig. 6C) and were likely responsible for the detected AOM-CH_4 activity, maintaining low environmental methane concentrations in these horizons (Fig. 2Q and R). ANME 2a-2c were also found in the 12.5–13.5 cm horizon, which was consistent with the dramatic increase in AOM activity in this horizon and the decline in methane (Fig. 2Q and R). The 16S rRNA analysis revealed that in this horizon, groups of methylotrophic and acetoclastic methanogens were detected alongside ANME's, suggesting coexistence of methanogens and ANME's in sediment horizons where sulfate reduction was also active (Fig. 2P). Interestingly, ANMEs were not detected between 13.5 and 19.5 cm despite the measurement of higher AOM activity (Fig. 2Q). Instead, several groups of methanogens extended into these deeper horizons, which could be linked to the higher methane concentrations found in these depths (Fig. 2R) as well as the higher levels of methane temporarily produced in methanogenesis batch incubations within deeper sections (Fig. 3C).

At the HP station, ANME 2a-2c families were found in the top 2.5 cm even though no AOM activity was detected by ^{14}C-CH_4 incubations in this layer. As the 16S data does not provide direct evidence of metabolic

activity, it is possible that the ANMEs were present but not active, potentially due to the high salinity in the HP station (Fig. 2V), causing osmotic stress and lowering or pausing AOM activity (Oren, 2011). In deeper sediment intervals, methanogenic families belonging to *Methanosarcinaceae* and *Methanonatronarchaeaceae* were detected. Both of these groups are halotolerant and can produce methane from non-competitive substrates and could be responsible for the methylotrophic methanogenesis activity we detected in the deeper sediments at the HP station (Boone et al., 2015; Sorokin et al., 2018).

An alternative hypothesis worth testing in future investigations is that methanogens are potentially responsible for mediating both methanogenesis and AOM in the cryptic methane cycle. Methanogens and ANMEs both carry the Mcr gene that encodes for the methyl coenzyme M, which depending on the thermodynamic conditions can work preferentially in either the reductive or oxidative directions (Hallam et al., 2003; Holler et al., 2011; Timmers et al., 2017). In addition, methanogenic groups within the *Methanosarcinales* order, which were detected in the CSMR sediments (Fig. 6) have been implicated in performing AOM coupled to iron reduction of poorly reactive iron oxides in lake sediment (Bar-Or et al., 2017) and in marine sediment (Liang et al., 2019; Yan et al., 2023; Yan et al., 2018). Testing the involvement of members of the *Methanosarcinales* in iron-dependent AOM could be particularly interesting for sediment intervals in which we detected simultaneous AOM activity (Fig. 2E, K, and Q), high porewater iron (II) concentrations (Fig. C, I, and O) and ASVs belonging to *Methanosarcinales* (Fig. 6A, B, C, and D). At the HP station, AOM was detected in deeper sediment intervals where no ANME ASVs were recovered. Here, AOM may also be mediated by groups of methanogens. At 16.5–17.5 cm, *Methanosarcinaceae*, was detected and could potentially contribute to the measured rates of AOM coupled to iron-reduction similar to the other stations. Indeed, Liu et al., (2025) found strong evidence that iron (III) is an important electron acceptor for AOM linked to cryptic methane cycling in the HP station. In combination, our data point to a potential involvement of methanogens in iron-dependent methane oxidation.

4.4. Indications for rapid turnover of metabolic substrates and non-methanogenic consumption of mono-methylamine

Salt marshes are known to be rich in fresh organic matter whose breakdown intermediates provide competitive and non-competitive substrates for methanogenesis (Fitzsimons et al., 2005; Fitzsimons et al., 1997; Wang and Lee, 1994; Yuan et al., 2014; Yuan et al., 2019). Porewater analysis by NMR revealed that porewaters from the BL, BH, and M stations had quantifiable concentrations of acetate. Acetate is a product from fermentation of organic matter by homoacetogenesis (Jørgensen, 2000; Ragsdale and Pierce, 2008). Acetate is an important substrate for a wide range of microbial groups and considered a competitive substrate between methanogenic archaea and sulfate-reducing bacteria (Conrad, 2020; Jørgensen, 2000). Acetate concentrations that were found to be below quantification or detection at our studied stations could point to rapid metabolic turnover, similar to what has been described for hydrogen (Conrad, 1999; Hoehler et al., 2001).

Porewater methanol was mostly below detection and sometimes present but not quantifiable in the CSMR sediment porewater (see section 3.1.5). Although methanol is known to be a non-competitive substrate for methylotrophic methanogenesis in coastal wetlands (King et al., 1983; Oremland and Polcin, 1982) it has recently been found to be a carbon source for non-methanogenic anaerobic methylotrophs such as denitrifying and sulfate-reducing bacteria (Fischer et al., 2021), which according to our 16S data are present in the CSMR (Figs. 5 and 7). As this substrate is expected to be produced in surface sediments of salt marshes (Oremland et al., 1982; Oremland and Polcin, 1982), low or undetectable concentrations of methanol in the porewater could indicate fast metabolic turnover, similar to acetate.

Natural porewater MMA concentrations were also mostly below detection (<3 μM), however, at some depth intervals in the BL and HP stations MMA concentrations were below quantification (<10 μM), but detectable (see section 3.1.5). It is not possible to report definitive quantities of MMA in this study; however, we can bracket the MMA concentrations in a range between 3 and 10 μM. MMA concentrations in sediment porewaters are still poorly constrained. A previous study of MMA in the Mersey Estuary, UK reports sediment porewater concentrations up to 319 μM (Fitzsimons et al., 1997). Other studies report lower sediment porewater concentrations, for example ~ 2 μM MMA in the Flax Pond salt marsh (Wang and Lee, 1994) and between 0.08 and 1.44 μM in the Thames Estuary, UK (Fitzsimons et al., 2006). Low MMA concentrations in the CSMR sediment porewater may as well indicate rapid metabolic consumption by the microbial community and/or binding to mineral surfaces (Wang and Lee, 1990; Xiao et al., 2022). Data from our ^{14}C-MMA incubations provide support for both hypotheses as we observed the metabolic potential for MMA through the turnover of the injected ^{14}C-MMA and found that between 38% and 55% of the injected ^{14}C-MMA bound to the sediment (see Sec. 3.3.1). Future investigations would benefit from methods that are sensitive enough to detect low quantities (i.e., <3 μM) of porewater MMA as well as the fraction of MMA bound to sediment surfaces to better quantify methylotrophic methanogenesis rates and thus cryptic methane cycling.

Interestingly, we found large differences between AOM-CH_4 (i.e., AOM determined based on ^{14}C-TIC production after injection of ^{14}C-CH_4) and AOM-MMA (AOM determined based on ^{14}C-TIC production after injection of ^{14}C-MMA) at all CSMR stations (Fig. 2E, K, Q, and W). In intervals where both AOM-CH_4 and AOM-MMA rates were detected, AOM-MMA was 1–2 orders of magnitude higher than AOM-CH_4 (Fig. 2E, K, Q, and W). We suggest the large difference between the two AOM rates is the result of ^{14}C-TIC production from direct oxidation of ^{14}C-MMA by non-methanogenic pathways, similar to what was previously hypothesized by Krause et al. (2023). Direct conversion of ^{14}C-MMA to ^{14}C-TIC would incorrectly inflate the rate constants for AOM-MMA dramatically (see Eq. (2)). Fig. 2F, L, R, and X indeed show that rate constants for AOM-MMA are 1–2 orders of magnitude higher than both MG-MMA and AOM-CH_4. We therefore suggest that the ^{14}C-TIC produced during the ^{14}C-MMA incubations stems only partially from AOM as part of the cryptic methane cycle (i.e., via the ^{14}C-CH_4 intermediate). The majority of ^{14}C-MMA was likely subject to direct methylamine oxidation by an unidentified anaerobic methylotrophic metabolism.

Methylamines are the simplest alkylated amine and derived from the degradation of osmolytes found in plant biomass (Oren, 1990; Taubert et al., 2017). Methylamines are ubiquitously found in saline and hypersaline conditions in marine sediments (Mausz and Chen, 2019; Zhuang et al., 2016; Zhuang et al., 2017) and in coastal wetlands (Fitzsimons et al., 2005; Fitzsimons et al., 1997; Fitzsimons et al., 2001; Fitzsimons et al., 2006). Because methylamine molecules are both a carbon and nitrogen source it is an important food source for a variety of microbial communities such as aerobic methylotrophic bacteria (Chistoserdova, 2015; Hanson and Hanson, 1996; Taubert et al., 2017) and obligate anaerobic methanogens (Chistoserdova, 2015; Thauer, 1998). However, increasing reports are providing evidence that methylamines may be directly oxidized anaerobically by non-methanogenic metabolisms in anoxic sediment (Cadena et al., 2018; De Anda et al., 2021; Farag et al., 2021; Kivenson et al., 2021; Zhuang et al., 2019). While this study does not directly identify the organisms responsible for non-methanogenic anaerobic mono-methylamine oxidation, our geochemical and molecular data suggest that sulfate-reducing bacteria may serve as potential mono-methylamine consumers in the CSMR, alongside methylotrophic methanogens. Kivenson et al., (2021) recently reanalyzed the metagenomes and metatranscriptomes of Desulfobacterales collected from sulfidic sediment in the Baltic Sea (Thureborn et al., 2016) and the Columbia River Estuary (Smith et al., 2015; Smith et al., 2019) and found the expression of trimethylamine metabolisms in the Desulfobacterales which strongly suggests that sulfate reducers could be actively in competition with methylotrophic methanogens. As Desulfobacterales were detected

throughout the sediment intervals across the CSMR transect (Fig. 7), it is possible that members of this group were actively involved in anaerobic methylamine consumption. Future research should investigate with transcriptomic studies to assess if sulfate-reducing lineages in the CSMR sediment are expressing the metabolic machinery required to utilize methylamines.

Our 16S rRNA data also revealed other archaeal and bacterial candidates that could potentially be implicated in methylamine consumption in the CSMR. At the BL and BH station, we detected both Bathyarchaeia and Lokiarchaeia (Fig. 5A and B). Metabolic reconstructions from metagenomes found that members of both groups have the potential for non-methanogenic anaerobic turnover of C1 compounds such as methanol and methylamines (Hou et al., 2023; Sun et al., 2021). Potential bacterial candidates for anaerobic methylamine oxidation in the CSMR transect are Proteobacteria, Firmicutes, Actinobacteria, Verrucomicrobia, candidate phylum NC10, and Actinobacteriota (Fig. 5E-H) as these phyla comprise known methylotrophs (Anthony, 1982; Chistoserdova and Lidstrom, 2013; McTaggart et al., 2015; Zemskaya et al., 2021).

If methylated substrates in anaerobic metabolism are not restricted to putative methanogenic archaea, then it is crucial to understand how competitive these substrates are between methylotrophic methanogens and other microorganisms. A hypothesis worth testing is that sulfate-reducing methylotrophs limit the availability of methylated substrates to methylotrophic methanogenesis in coastal wetland sediment. If confirmed by future studies, this process could help explain the relatively low methane emissions from coastal wetlands and contribute to refining estimates of the global methane budget. Identifying this unknown metabolism, the responsible microbial groups, and the competition mechanism is crucial. If environmental conditions shift to favor methanogenic archaea, it remains unclear whether the existing cryptic methane cycle will be amplified or if coastal wetlands will become a larger methane source.

4.5. Implications for cryptic methane cycling in coastal wetlands

Coastal wetlands are at the boundary between terrestrial and marine ecosystems. However, reports showing the decline in coastal wetland areas due to a variety of anthropogenic pressures (i.e., land reclamation, agriculture, and run off) are increasing (Newton et al., 2020). The leading concern is sea-level rise caused by increasing temperatures globally driven by climate change. The fear is that sea-level rise will potentially permanently inundate coastal wetland areas globally. This inundation of seawater could affect the coastal wetland water tables and deliver more organic material into coastal wetlands, leading to changes in biogeochemical cycles and uncertainties in methane emissions from coastal wetland systems (Chambers et al., 2013; Ding et al., 2010; Dinsmore et al., 2009; Gatland et al., 2014; Liu et al., 2019; Vizza et al., 2017; Wei et al., 2020; Xu et al., 2021; Zhao et al., 2020). As this imminent issue emerges, important questions remain regarding the response of anaerobic methylotrophic activity and cryptic methane cycling to climate-driven sea-level rise in coastal wetlands. Such inundations could promote cryptic methane cycling, driven by large pools of electron acceptors in the sediment porewaters, helping to maintain low methane concentrations and thereby regulate the emission of this potent greenhouse gas.

5. Conclusions

In the present study, we set about to find spatial evidence of cryptic methane cycling and the potential microbial communities involved in the surface sediments along a land–ocean, 4-station transect within a southern Californian salt marsh. We found spatial overlap of methylotrophic methanogenesis and AOM activity in different depth horizons at all four stations. We also observed spatial variability between sulfate reduction, methylotrophic methanogenesis and AOM activities across the CSMR transect. Particularly, we found that the brackish portions of the CSMR AOM played a minor role in this area but concurrent sulfate reduction and methylotrophic methanogenesis activities were detected, along with higher abundances of known groups of methanogens and sulfate reducers. Whereas higher AOM activity, along with higher abundances of microbial groups known to perform AOM, overlapped with methylotrophic methanogenesis activity at the Marine and Hypersaline pool stations. We conclude that the cryptic methane cycle is active keeping methane concentrations present but low across the salt marsh transect.

We further found that the salinity at the sediment–water interface of the supposedly brackish stations was different from the subsurface, where high salinity and high availability of sulfate prevailed, suggesting that more inland portions of the saltmarsh may have once been more hypersaline. At none of the four stations sulfate was limiting in the subsurface, supporting sulfate reduction activity, which was in part likely linked to AOM in cryptic methane cycling. However, the concomitant presence of porewater iron (II) and genetic evidence of the presence of heterotrophic iron-reducing bacteria as well as ANME known to couple methane oxidation with iron reduction, indicate that iron (III) too, could be an important electron acceptor in this environment for both organic matter degradation and AOM.

Metabolomic analysis of porewater indicate a rapid production and consumption of methanogenic substrates, including acetate, methanol, and MMA. While molecular data revealed methanogenic archaea at all stations, ANME were present only at the marine and hypersaline stations. This finding suggest that cryptic methane cycling could be facilitated by either a methanogen-methanotroph archaea couple, where both groups coincided, or by putative methanogenic archaea capable of both processes, where ANME were absent. Our data from radioisotope incubations strongly suggest that not only is cryptic methane cycling active in the salt marsh sediment, but there is also an unknown anaerobic methylotrophic metabolism directly oxidizing methylamine into the inorganic carbon pool. Our molecular and biogeochemical analyses along with literature evidence identified sulfate-reducing bacteria as a potential candidate responsible for the turnover of methylated substrates, but more work is needed to confirm.

Our study emphasizes the biogeochemical complexity occurring in the sediment across spatial gradients within a salt marsh. Based on the overwhelming abundance of electron acceptors for AOM and the presence of microbial communities capable of cycling methane or suppressing competitive methanogenesis pathways within the sediment across the CSMR transect, the findings in this study indicate that the surface sediment within salt marshes like the CSMR might already be primed to handle potential enhanced methane production caused by climate change induced sea-level rise.

Declaration of generative AI and AI-assisted technologies in the writing process

During the revision of the manuscript the authors used ChatGPT to improve conciseness and readability. After using this AI tool, the authors reviewed and edited the content as needed and take full responsibility for the content of the publication.

Data availability

Datasets from geochemical and radiotracer (i.e., ^{14}C and ^{35}S) analysis are accessible via the Biological and Chemical Oceanography Data Management Office (BCO-DMO) database DOI: https://www.bco-dmo.org/dataset/965250. Data from the 16S rRNA molecular analysis are accessible via the National Center for Biotechnology Information (NCBI) Bio Project https://www.ncbi.nlm.nih.gov/bioproject/PRJNA1199032.

CRediT authorship contribution statement

Sebastian J.E. Krause: Writing – original draft, Visualization, Validation, Supervision, Project administration, Methodology, Investigation, Formal analysis, Data curation, Conceptualization. **Rebecca Wipfler:** Writing – review & editing, Visualization, Validation, Software, Methodology, Formal analysis. **Jiarui Liu:** Writing – review & editing, Investigation. **David J. Yousavich:** Writing – review & editing, Investigation. **DeMarcus Robinson:** Writing – review & editing, Investigation. **David W. Hoyt:** Writing – review & editing, Resources, Investigation, Formal analysis. **Victoria J. Orphan:** Writing – review & editing, Supervision, Resources, Investigation, Formal analysis. **Tina Treude:** Writing – review & editing, Validation, Resources, Project administration, Methodology, Funding acquisition, Data curation, Conceptualization.

Declaration of competing interest

The authors declare that they have no known competing financial interests or personal relationships that could have appeared to influence the work reported in this paper.

Acknowledgements

The authors thank the University of California Natural Reserve System and the Project Scientist of the Carpinteria Salt Marsh Reserve, A. Brooks, for authorizing the field sampling in June 2019. We acknowledge X. Hwang for providing fieldwork and laboratory instrument support. We acknowledge S. Connon and S. Lim for providing laboratory and sequencing analysis support. This work received financial support through the University of California and the National Science Foundation (NSF) (Award No.: 1852912). The NMR experiments in this study were performed under a limited scope project awarded (proposal 51757: 10.46936/ltds.proj.2020.51757/60006896) to T. Treude using the Environmental Molecular Sciences Laboratory, a DOE Office of Science User Facility sponsored by the Biological and Environmental Research program under Contract No. DE-AC05-76RL01830. J. Liu was supported by the NASA FINESST Fellowship 80NSSC21K1529. V. J. Orphan and R. Wipfler contributions were supported through the U.S. Department of Energy, Office of Science, Office of Biological and Environmental Research under Award Number DE-SC0022991.

References

Anthony, C., 1982. The biochemistry of methylotrophs.
Aromokeye, D.A., Kulkarni, A.C., Elvert, M., Wegener, G., Henkel, S., Coffinet, S., Eickhorst, T., Oni, O.E., Richter-Heitmann, T., Schnakenberg, A., 2020. Rates and microbial players of iron-driven anaerobic oxidation of methane in methanic marine sediments. Front. Microbiol. 10, 487993.
Bar-Or, I., Elvert, M., Eckert, W., Kushmaro, A., Vigderovich, H., Zhu, Q., Ben-Dov, E., Sivan, O., 2017. Iron-coupled anaerobic oxidation of methane performed by a mixed bacterial-archaeal community based on poorly reactive minerals. Environ. Sci. Technol. 51 (21), 12293–12301.
Barnes, R.O., Goldberg, E.D., 1976. Methane production and consumption in anoxic marine sediments. Geology 4, 297–300.
Bartlett, K.B., Bartlett, D.S., Harriss, R.C., Sebacher, D.J., 1987. Methane emissions along a salt marsh salinity gradient. Biogeochemistry 4, 183–202.
Beal, E.J., House, C.H., Orphan, V.J., 2009. Manganese- and iron-dependent marine methane oxidation. Science 325, 184–187.
Bernard, B.B., 1979. Methane in marine sediments. Deep Sea Res. Part A 26 (4), 429–443.
Beulig, F., Røy, H., McGlynn, S.E., Jørgensen, B.B., 2018. Cryptic CH_4 cycling in the sulfate-methane transition of marine sediments apparently mediated by ANME-1 archaea. ISME J.
Boetius, A., Ravenschlag, K., Schubert, C.J., Rickert, D., Widdel, F., Giesecke, A., Amann, R., Jørgensen, B.B., Witte, U., Pfannkuche, O., 2000. A marine microbial consortium apparently mediating anaerobic oxidation of methane. Nature 407, 623–626.
Booij, K., Helder, W., Sundby, B., 1991. Rapid redistribution of oxygen in a sandy sediment induced by changes in the flow velocity of the overlying water. Neth. J. Sea Res. 28 (3), 149–165.
Boone, D.R., Whitman, W.B., Koga, Y., 2015. Methanosarcinaceae. Bergey's Man. Syst. Archaea Bacteria 1–2.
Boudreau, B.P., Huettel, M., Forster, S., Jahnke, R.A., McLachlan, A., Middelburg, J.J., Nielsen, P., Sansone, F., Taghon, G., Van Raaphorst, W., 2001. Permeable marine sediments: overturning an old paradigm. Eos Trans. AGU 82 (11), 133–136.
Bueno de Mesquita, C.P., Wu, D., Tringe, S.G., 2023. Methyl-based methanogenesis: an ecological and genomic review. Microbiol. Mol. Biol. Rev. 87 (1), e00024–e122.
Cadena, S., García-Maldonado, J.Q., López-Lozano, N.E., Cervantes, F.J., 2018. Methanogenic and sulfate-reducing activities in a hypersaline microbial mat and associated microbial diversity. Microb. Ecol. 75 (4), 930–940.
Callahan, B.J., McMurdie, P.J., Rosen, M.J., Han, A.W., Johnson, A.J.A., Holmes, S.P., 2016. DADA2: high-resolution sample inference from Illumina amplicon data. Nat. Methods 13 (7), 581–583.
Cao, M., Xin, P., Jin, G., Li, L., 2012. A field study on groundwater dynamics in a salt marsh–Chongming Dongtan wetland. Ecol. Eng. 40, 61–69.
Carol, E.S., Dragani, W.C., Kruse, E.E., Pousa, J.L., 2012. Surface water and groundwater characteristics in the wetlands of the Ajó River (Argentina). Cont. Shelf Res. 49, 25–33.
Carol, E.S., Kruse, E.E., Pousa, J.L., 2011. Influence of the geologic and geomorphologic characteristics and of crab burrows on the interrelation between surface water and groundwater in an estuarine coastal wetland. J. Hydrol. 403 (3–4), 234–241.
Chadwick, G.L., Skennerton, C.T., Laso-Pérez, R., Leu, A.O., Speth, D.R., Yu, H., Morgan-Lang, C., Hatzenpichler, R., Goudeau, D., Malmstrom, R., 2022. Comparative genomics reveals electron transfer and syntrophic mechanisms differentiating methanotrophic and methanogenic archaea. PLoS Biol. 20 (1), e3001508.
Chambers, L.G., Osborne, T.Z., Reddy, K.R., 2013. Effect of salinity-altering pulsing events on soil organic carbon loss along an intertidal wetland gradient: a laboratory experiment. Biogeochemistry 115, 363–383.
Chistoserdova, L., 2015. Methylotrophs in natural habitats: current insights through metagenomics. Appl. Microbiol. Biotechnol. 99 (14), 5763–5779.
Chistoserdova, L., Lidstrom, M.E., 2013. Aerobic methylotrophic prokaryotes. The Prokaryotes 267–285.
Cline, J.D., 1969. Spectrophometric determination of hydrogen sulfide in natural waters. Limnol. Oceanogr. 14, 454–458.
Conrad, R., 1999. Contribution of hydrogen to methane production and control of hydrogen concentrations in methanogenic soils and sediments. FEMS Microbiol. Ecol. 28 (3), 193–202.
Conrad, R., 2020. Importance of hydrogenotrophic, aceticlastic and methylotrophic methanogenesis for methane production in terrestrial, aquatic and other anoxic environments: a mini review. Pedosphere 30 (1), 25–39.
Cui, S., Liu, P., Guo, H., Nielsen, C.K., Pullens, J.W.M., Chen, Q., Pugliese, L., Wu, S., 2024. Wetland hydrological dynamics and methane emissions. Commun. Earth Environ. 5 (1), 470.
Dale, A.W., Sommer, S., Lomnitz, U., Montes, I., Treude, T., Liebetrau, V., Gier, J., Hensen, C., Dengler, M., Stolpovsky, K., Bryant, L.D., Wallmann, K., 2015. Organic carbon production, mineralisation and preservation on the Peruvian margin. Biogeosciences 12, 1537–1559.
De Anda, V., Chen, L.-X., Dombrowski, N., Hua, Z.-S., Jiang, H.-C., Banfield, J.F., Li, W.-J., Baker, B.J., 2021. Brockarchaeota, a novel archaeal phylum with unique and versatile carbon cycling pathways. Nat. Commun. 12 (1), 1–12.
del Pilar Alvarez, M., Carol, E., Hernández, M.A., Bouza, P.J., 2015. Groundwater dynamic, temperature and salinity response to the tide in Patagonian marshes: observations on a coastal wetland in San José Gulf, Argentina. J. S. Am. Earth Sci. 62, 1–11.
Diao, M., Dyksma, S., Koeksoy, E., Ngugi, D.K., Anantharaman, K., Loy, A., Pester, M., 2023. Global diversity and inferred ecophysiology of microorganisms with the potential for dissimilatory sulfate/sulfite reduction. FEMS Microbiol. Rev. 47 (5) fuad058.
Ding, W., Zhang, Y., Cai, Z., 2010. Impact of permanent inundation on methane emissions from a Spartina alterniflora coastal salt marsh. Atmos. Environ. 44 (32), 3894–3900.
Dinsmore, K.J., Skiba, U.M., Billett, M.F., Rees, R.M., 2009. Effect of water table on greenhouse gas emissions from peatland mesocosms. Plant and Soil 318, 229–242.
Dong, W., Zhou, J., Zhang, C.-J., Yang, Q., Li, M., 2024. Methylotrophic substrates stimulated higher methane production than competitive substrates in mangrove sediments. Sci. Total Environ. 951, 175677.
Egger, M., Hagens, M., Sapart, C.J., Dijkstra, N., van Helmond, N.A., Mogollón, J.M., Risgaard-Petersen, N., van der Veen, C., Kasten, S., Riedinger, N., 2017. Iron oxide reduction in methane-rich deep Baltic Sea sediments. Geochim. Cosmochim. Acta 207, 256–276.
Egger, M., Rasigraf, O., Sapart, C.J., Jilbert, T., Jetten, M.S., Rockmann, T., Van der Veen, C., Banda, N., Kartal, B., Ettwig, K.F., 2015. Iron-mediated anaerobic oxidation of methane in brackish coastal sediments. Environ. Sci. Technol. 49 (1), 277–283.
Ettwig, K.F., Zhu, B., Speth, D., Keltjens, J.T., Jetten, M.S., Kartal, B., 2016. Archaea catalyze iron-dependent anaerobic oxidation of methane. P. Natl. Acad. Sci. USA 113 (45), 12792–12796.
Evans, P.N., Parks, D.H., Chadwick, G.L., Robbins, S.J., Orphan, V.J., Golding, S.D., Tyson, G.W., 2015. Methane metabolism in the archaeal phylum Bathyarchaeota revealed by genome-centric metagenomics. Science 350 (6259), 434–438.
Farag, I.F., Zhao, R., Biddle, J.F., 2021. "Sifarchaeota," a novel asgard phylum from Costa Rican sediment capable of polysaccharide degradation and anaerobic methylotrophy. Appl. Environ. Microbiol. 87 (9), e02584–02520.
Fischer, P.Q., Sánchez-Andrea, I., Stams, A.J., Villanueva, L., Sousa, D.Z., 2021. Anaerobic microbial methanol conversion in marine sediments. Environ. Microbiol. 23 (3), 1348–1362.

Fitzsimons, M., Dawit, M., Revitt, D., Rocha, C., 2005. Effects of early tidal inundation on the cycling of methylamines in inter-tidal sediments. Mar. Ecol. Prog. Ser. 294, 51–61.
Fitzsimons, M.F., Jemmett, A.W., Wolff, G.A., 1997. A preliminary study of the geochemistry of methylamines in a salt marsh. Org Geochem. 27 (1–2), 15–24.
Fitzsimons, M.F., Kahni-danon, B., Dawitt, M., 2001. Distributions and adsorption of the methylamines in the inter-tidal sediments of an East Anglian Estuary. Environ. Exp. Bot. 46, 225–236.
Fitzsimons, M.F., Millward, G.E., Revitt, D.M., Dawit, M.D., 2006. Desorption kinetics of ammonium and methylamines from estuarine sediments: consequences for the cycling of nitrogen. Mar. Chem. 101 (1–2), 12–26.
Gao, Y., Wang, Y., Lee, H.-S., Jin, P., 2022. Significance of anaerobic oxidation of methane (AOM) in mitigating methane emission from major natural and anthropogenic sources: a review of AOM rates in recent publications. Environ. Sci.: Adv. 1 (4), 401–425.
Gardner, L.R., 2007. Role of stratigraphy in governing pore water seepage from salt marsh sediments. Water Resour. Res. 43 (7).
Gatland, J.R., Santos, I.R., Maher, D.T., Duncan, T., Erler, D.V., 2014. Carbon dioxide and methane emissions from an artificially drained coastal wetland during a flood: implications for wetland global warming potential. J. Geophys. Res. Biogeo. 119 (8), 1698–1716.
Grasshoff, K., Ehrhardt, M., Kremling, K., 1999. Methods of seawater analysis. Wiley-VCH Verlag GmbH, Weinheim.
Gribsholt, B., Kristensen, E., 2002. Effects of bioturbation and plant roots on salt marsh biogeochemistry: a mesocosm study. Mar. Ecol. Prog. Ser. 241, 71–87.
Hallam, S.J., Girguis, P.R., Preston, C.M., Richardson, P.M., DeLong, E.F., 2003. Identification of methyl coenzym m reductase A (mcrA) genes associated with methane-oxidizing archaea. Appl. Environ. Microbiol. 69 (9), 5483–5491.
Hansel, C.M., Lentini, C.J., Tang, Y., Johnston, D.T., Wankel, S.D., Jardine, P.M., 2015. Dominance of sulfur-fueled iron oxide reduction in low-sulfate freshwater sediments. ISME J. 9 (11), 2400–2412.
Hanson, R.S., Hanson, T.E., 1996. Methanotrophic bacteria. Microbiol. Rev. 60 (2), 439–471.
Harris, D., Horwáth, W.R., Van Kessel, C., 2001. Acid fumigation of soils to remove carbonates prior to total organic carbon or carbon-13 isotopic analysis. Soil Sci. Soc. Am. J. 65 (6), 1853–1856.
Hinrichs, K.-U., Boetius, A., 2002. The anaerobic oxidation of methane: new insights in microbial ecology and biogeochemistry. In: Wefer, G., Billett, D., Hebbeln, D., Jørgensen, B.B., Schlüter, M., Van Weering, T. (Eds.), Ocean Margin Systems. Springer-Verlag, Berlin, pp. 457–477.
Hoehler, T.M., Alperin, M.J., Albert, D.B., Martens, C.S., 2001. Apparent minimum free energy requirements for methanogenic Archaea and sulfate-reducing bacteria in an anoxic marine sediment. FEMS Microbiol. Ecol. 38, 33–41.
Holler, T., Wegener, G., Niemann, H., Deusner, C., Ferdelman, T.G., Boetius, A., Brunner, B., Widdel, F., 2011. Carbon and sulfur back flux during anaerobic microbial oxidation of methane and coupled sulfate reduction. Proc. Natl. Acad. Sci. 108 (52). E1484-E1490.
Holmer, M., Kristensen, E., Banta, G., Hansen, K., Jensen, M.H., Bussawarit, N., 1994. Biogeochemical cycling of sulfur and iron in sediments of a south-east Asian mangrove, Phuket Island, Thailand. Biogeochemistry 26, 145–161.
Holmes, D.E., Nicoll, J.S., Bond, D.R., Lovley, D.R., 2004. Potential role of a novel psychrotolerant member of the family geobacteraceae, geopsychrobacter electrodiphilus gen. nov., sp. nov., in electricity production by a marine sediment fuel cell. Appl. Environ. Microbiol. 70 (10), 6023–6030.
Hou, J., Wang, Y., Zhu, P., Yang, N., Liang, L., Yu, T., Niu, M., Konhauser, K., Woodcroft, B.J., Wang, F., 2023. Taxonomic and carbon metabolic diversification of Bathyarchaeia during its coevolution history with early Earth surface environment. Sci. Adv. 9 (27), eadf5069.
Huettel, M., Ziebis, W., Forster, S., 1996. Flow-induced uptake of particulate matter in permeable sediments. Limnol. Oceanogr. 41 (2), 309–322.
Huettel, M., Ziebis, W., Forster, S., Luther, I.G.W., 1998. Advective transport affecting metal and nutrient distribution and interfacial fluxes in permeable sediments. Geochim. Cosmochim. Acta 62 (4), 613–631.
Hyun, J.-H., Smith, A.C., Kostka, J.E., 2007. Relative contributions of sulfate-and iron (III) reduction to organic matter mineralization and process controls in contrasting habitats of the Georgia saltmarsh. Appl. Geochem. 22 (12), 2637–2651.
IPCC, 2021. Climate Change 2021 – The Physical Science Basis: Working Group I Contribution to the Sixth Assessment Report of the Intergovernmental Panel on Climate Change. Cambridge: Cambridge University Press.
Iversen, N., Jørgensen, B.B., 1993. Diffusion coefficients of sulfate and methane in marine sediments: influence of porosity. Geochim. Cosmochim. Acta 57, 571–578.
Jackson, K.L., Whitcraft, C.R., Dillon, J.G., 2014. Diversity of Desulfobacteriaceae and overall activity of sulfate-reducing microorganisms in and around a salt pan in a southern California coastal wetland. Wetlands 34, 969–977.
Joye, S.B., Boetius, A., Orcutt, B.N., Montoya, J.P., Schulz, H.N., Erickson, M.J., Logo, S. K., 2004. The anaerobic oxidation of methane and sulfate reduction in sediments from Gulf of Mexico cold seeps. Chem. Geol. 205, 219–238.
Jørgensen, B.B., 2000. Bacteria and marine biogeochemistry. In: Schulz, H.D., Zabel, M. (Eds.), Marine Biogeochemistry. Springer Verlag, Berlin, pp. 173–201.
Kallmeyer, J., Ferdelman, T.G., Weber, A., Fossing, H., Jørgensen, B.B., 2004. A cold chromium distillation procedure for radiolabeled sulfide applied to sulfate reduction measurements. Limnol. Oceanogr. Methods 2, 171–180.
King, G., Klug, M.J., Lovley, D.R., 1983. Metabolism of acetate, methanol, and methylated amines in intertidal sediments of Lowes Cove. Maine 45 (6), 1848–1853.
Kivenson, V., Paul, B.G., Valentine, D.L., 2021. An ecological basis for dual genetic code expansion in marine deltaproteobacteria. Front. Microbiol. 1545.
Knittel, K., Boetius, A., 2009. Anaerobic oxidation of methane: progress with an unknown process. Annu. Rev. Microbiol. 63, 311–334.
Knittel, K., Wegener, G., Boetius, A., 2018. Anaerobic methane oxidizers. Microbial communities utilizing hydrocarbons and lipids: members. In: McGenity, T.J. (Ed.), Metagenomics and Ecophysiology. Springer, Cham, pp. 1–21.
Knudsen, M., 1901. Hydrographical tables according to the measurings of Carl Forch...[et Al.] and with assistance of Björn-Andersen...[et Al.]. GEC Gad.
Koretsky, C.M., Moore, C.M., Lowe, K.L., Meile, C., DiChristina, T.J., Van Cappellen, P., 2003. Seasonal oscillation of microbial iron and sulfate reduction in saltmarsh sediments (Sapelo Island, GA, USA). Biogeochemistry 64 (2), 179–203.
Kostka, J.E., Roychoudhury, A., Van Cappellen, P., 2002. Rates and controls of anaerobic microbial respiration across spatial and temporal gradients in saltmarsh sediments. Biogeochemistry 60, 49–76.
Krause, S.J., Liu, J., Yousavich, D.J., Robinson, D., Hoyt, D.W., Qin, Q., Wenzhöfer, F., Janssen, F., Valentine, D.L., Treude, T., 2023. Evidence of cryptic methane cycling and non-methanogenic methylamine consumption in the sulfate-reducing zone of sediment in the Santa Barbara Basin, California. Biogeosciences 20 (20), 4377–4390.
Krause, S.J., Treude, T., 2021. Deciphering cryptic methane cycling: coupling of methylotrophic methanogenesis and anaerobic oxidation of methane in hypersaline coastal wetland sediment. Geochim. Cosmochim. Acta 302, 160–174.
Kristjansson, J.K., Schönheit, P., Thauer, R.K., 1982. Different Ks values for hydrogen of methanogenic bacteria and sulfate reducing bacteria: an explanation for the apparent inhibition of methanogenesis by sulfate. Arch. Microbiol. 131, 278–282.
La, W., Han, X., Liu, C.-Q., Ding, H., Liu, M., Sun, F., Li, S., Lang, Y., 2022. Sulfate concentrations affect sulfate reduction pathways and methane consumption in coastal wetlands. Water Res. 217, 118441.
Lapham, L.L., Lloyd, K.G., Fossing, H., Flury, S., Jensen, J.B., Alperin, M.J., Rehder, G., Holzhueter, W., Ferdelman, T., Jørgensen, B.B., 2024. Methane leakage through the sulfate–methane transition zone of the Baltic seabed. Nat. Geosci. 17 (12), 1277–1283.
Lentini, C.J., Wankel, S.D., Hansel, C.M., 2012. Enriched iron (III)-reducing bacterial communities are shaped by carbon substrate and iron oxide mineralogy. Front. Microbiol. 3, 404.
Leu, A.O., Cai, C., McIlroy, S.J., Southam, G., Orphan, V.J., Yuan, Z., Hu, S., Tyson, G.W., 2020. Anaerobic methane oxidation coupled to manganese reduction by members of the Methanoperedenaceae. ISME J. 14 (4), 1030–1041.
Li, Y., Wang, D., Chen, Z., Chen, J., Hu, H., Wang, R., 2021. Methane emissions during the tide cycle of a Yangtze Estuary salt marsh. Atmos. 12 (2), 245.
Li, Z., Hodges, B.R., Shen, X., 2023. Modeling hypersalinity caused by evaporation and surface–subsurface exchange in a coastal marsh. J. Hydrol. 618, 129268.
Liang, L., Wang, Y., Sivan, O., Wang, F., 2019. Metal-dependent anaerobic methane oxidation in marine sediment: insights from marine settings and other systems. Sci. China Life Sci. 62, 1287–1295.
Lin, C.Y., Turchyn, A.V., Krylov, A., Antler, G., 2020. The microbially driven formation of siderite in salt marsh sediments. Geobiology 18 (2), 207–224.
Liu, J., Klonicki-Ference, E., Krause, S.J., Treude, T., 2025. Iron oxides fuel anaerobic oxidation of methane in the presence of sulfate in hypersaline coastal wetland sediment. Environ. Sci. Technol. 59 (1), 513–522.
Liu, L., Wang, D., Chen, S., Yu, Z., Xu, Y., Li, Y., Ge, Z., Chen, Z., 2019. Methane emissions from estuarine coastal wetlands: implications for global change effect. Soil Sci. Soc. Am. J. 83 (5), 1368–1377.
Liu, Y., Whitman, W.B., 2008. Metabolic, phylogenetic, and ecological diversity of the methanogenic archaea. Ann. N. Y. Acad. Sci. 1125 (1), 171–189.
Lovley, D.R., Klug, M.J., 1986. Model for the distribution of sulfate reduction and methanogenesis in freshwater sediments. Geochim. Cosmochim. Acta 50, 11–18.
Lovley, D.R., Phillips, E.J., 1987. Competitive mechanisms for inhibition of sulfate reduction and methane production in the zone of ferric iron reduction in sediments. Appl. Environ. Microbiol. 53 (11), 2636–2641.
López-Archilla, A.I., Moreira, D., Velasco, S., López-García, P., 2007. Archaeal and bacterial community composition of a pristine coastal aquifer in Donana National Park, Spain. Aquatic Microbial. Ecol. 47 (2), 123–139.
Maltby, J., Sommer, S., Dale, A., Treude, T., 2016. Microbial methanogenesis in the sulfate-reducing zone of surface sediments traversing the Peruvian margin. Biogeosciences 13 (1), 283–299.
Martin, M., 2011. Cutadapt removes adapter sequences from high-throughput sequencing reads. Embnet. Journal 17 (1), 10–12.
Martinez-Cruz, K., Sepulveda-Jauregui, A., Casper, P., Anthony, K.W., Smemo, K.A., Thalasso, F., 2018. Ubiquitous and significant anaerobic oxidation of methane in freshwater lake sediments. Water Res. 144, 332–340.
Mausz, M.A., Chen, Y., 2019. Microbiology and ecology of methylated amine metabolism in marine ecosystems. Curr. Issues Mol. Biol. 33 (1), 133–148.
McTaggart, T.L., Beck, D.A., Setboonsarng, U., Shapiro, N., Woyke, T., Lidstrom, M.E., Kalyuzhnaya, M.G., Chistoserdova, L., 2015. Genomics of methylotrophy in Gram-positive methylamine-utilizing bacteria. Microorganisms 3 (1), 94–112.
Michaelis, W., Seifert, R., Nauhaus, K., Treude, T., Thiel, V., Blumenberg, M., Knittel, K., Gieseke, A., Peterknecht, K., Pape, T., Boetius, A., Aman, A., Jørgensen, B.B., Widdel, F., Peckmann, J., Pimenov, N.V., Gulin, M., 2002. Microbial reefs in the Black Sea fueled by anaerobic oxidation of methane. Science 297, 1013–1015.
Moffett, K.B., Robinson, D.A., Gorelick, S.M., 2010. Relationship of salt marsh vegetation zonation to spatial patterns in soil moisture, salinity, and topography. Ecosystems 13, 1287–1302.
Montalto, F.A., Steenhuis, T.S., Parlange, J.-Y., 2006. The hydrology of Piermont Marsh, a reference for tidal marsh restoration in the Hudson river estuary, New York. J. Hydrol. 316 (1–4), 108–128.

Motelica-Heino, M., Naylor, C., Zhang, H., Davison, W., 2003. Simultaneous release of metals and sulfide in lacustrine sediment. Environ. Sci. Technol. 37 (19), 4374–4381.
Murali, R., Yu, H., Speth, D.R., Wu, F., Metcalfe, K.S., Crémière, A., Laso-Pèrez, R., Malmstrom, R.R., Goudeau, D., Woyke, T., 2023. Physiological potential and evolutionary trajectories of syntrophic sulfate-reducing bacterial partners of anaerobic methanotrophic archaea. PLoS Biol. 21 (9), e3002292.
Newton, A., Icely, J., Cristina, S., Perillo, G.M., Turner, R.E., Ashan, D., Cragg, S., Luo, Y., Tu, C., Li, Y., 2020. Anthropogenic, direct pressures on coastal wetlands. Front. Ecol. Evol. 8, 144.
Oksanen, J., Simpson, G., Blanchet, F., Kindt, R., Legendre, P., Minchin, P., O'Hara, R., Solymos, P., Stevens, M., Szoecs, E., 2022. Vegan: Community Ecology Package. R package version 2.6-2. 2022. Google Scholar There is no corresponding record for this reference.
Oremland, R.S., Marsh, L.M., Polcin, S., 1982. Methane production and simultaneous sulphate reduction in anoxic, salt marsh sediments. Nature 296, 143–145.
Oremland, R.S., Polcin, S., 1982. Methanogenesis and sulfate reduction: competitive and noncompetitive substrates in estuarine sediments. Appl. Environ. Microbiol. 44 (6), 1270–1276.
Oremland, R.S., Taylor, B.F., 1978. Sulfate reduction and methanogenesis in marine sediments. Geochim. Cosmochim. Acta 42 (2), 209–214.
Oren, A., 1990. Formation and breakdown of glycine betaine and trimethylamine in hypersaline environments. Antonie Van Leeuwenhoek 58, 291–298.
Oren, A., 2011. Thermodynamic limits to microbial life at high salt concentrations. Environ. Microbiol. 13 (8), 1908–1923.
Oren, A., 2014. The family methanoregulaceae. The Prokaryotes: Other Major Lineages Bacteria Archaea 253–258.
Orphan, V.J., Hinrichs, K.-U., Ussler III, W., Paull, C.K., Tayleor, L.T., Sylva, S.P., Hayes, J.M., DeLong, E.F., 2001a. Comparative analysis of methane-oxidizing archaea and sulfate-reducing bacteria in anoxic marine sediments. Appl. Environ. Microbiol. 67 (4), 1922–1934.
Orphan, V.J., House, C.H., Hinrichs, K.-U., McKeegan, K.D., De Long, E.F., 2001b. Methane-consuming Archaea revealed by directly coupled isotopic and phylogenetic analysis. Science 293, 484–487.
Park, H.S., Lin, S., Voordouw, G., 2008. Ferric iron reduction by Desulfovibrio vulgaris Hildenborough wild type and energy metabolism mutants. Antonie Van Leeuwenhoek 93, 79–85.
Parkes, R.J., Brock, F., Banning, N., Hornibrook, E.R., Roussel, E.G., Weightman, A.J., Fry, J.C., 2012. Changes in methanogenic substrate utilization and communities with depth in a salt-marsh, creek sediment in southern England. Estuar. Coast. Shelf Sci. 96, 170–178.
Postma, D., Jakobsen, R., 1996. Redox zonation: equilibrium constraints on the Fe (III)/SO_4-reduction interface. Geochim. Cosmochim. Acta 60 (17), 3169–3175.
Poulton, S.W., Krom, M.D., Raiswell, R., 2004. A revised scheme for the reactivity of iron (oxyhydr) oxide minerals towards dissolved sulfide. Geochim. Cosmochim. Acta 68 (18), 3703–3715.
Precht, E., Franke, U., Polerecky, L., Huettel, M., 2004. Oxygen dynamics in permeable sediments with wave-driven pore water exchange. Limnol. Oceanogr. 49 (3), 693–705.
Quast, C., Pruesse, E., Yilmaz, P., Gerken, J., Schweer, T., Yarza, P., Peplies, J., Glöckner, F.O., 2012. The SILVA ribosomal RNA gene database project: improved data processing and web-based tools. Nucleic Acids Res. 41 (D1). D590-D596.
Ragsdale, S.W., Pierce, E., 2008. Acetogenesis and the Wood–Ljungdahl pathway of CO_2 fixation. Biochimica et Biophysica Acta (BBA)-Proteins Proteomics 1784 (12), 1873–1898.
Raiswell, R., Berner, R.A., 1985. Pyrite formation in euxinic and semi-euxinic sediments. Am. J. Sci. 285, 710–724.
Reddy, K.R., DeLaune, R.D., 2008. Biogeochemistry of Wetlands. CRC Press, Taylor & Francis Group, Boca Raton.
Reddy, K.R., DeLaune, R.D., Inglett, P.W., 2022. Biogeochemistry of wetlands: science and applications. CRC Press.
Reeburgh, W.S., 2007. Oceanic methane biogeochemistry. Chem. Rev. 107 (2), 486–513.
Reyes, C., Schneider, D., Thürmer, A., Kulkarni, A., Lipka, M., Sztejrenszus, S.Y., Böttcher, M.E., Daniel, R., Friedrich, M.W., 2017. Potentially active iron, sulfur, and sulfate reducing bacteria in Skagerrak and Bothnian Bay sediments. Geomicrobiol J. 34 (10), 840–850.
Rocha, C., 1998. Rhythmic ammonium regeneration and flushing in intertidal sediments of the Sado estuary. Limnol. Oceanogr. 43 (5), 823–831.
Rooze, J., Egger, M., Tsandev, I., Slomp, C.P., 2016. Iron-dependent anaerobic oxidation of methane in coastal surface sediments: potential controls and impact. Limnol. Oceanogr. 61 (S1). S267-S282.
Rosentreter, J.A., Borges, A.V., Deemer, B.R., Holgerson, M.A., Liu, S., Song, C., Melack, J., Raymond, P.A., Duarte, C.M., Allen, G.H., 2021. Half of global methane emissions come from highly variable aquatic ecosystem sources. Nat. Geosci. 14 (4), 225–230.
Rosentreter, J.A., Laruelle, G.G., Bange, H.W., Bianchi, T.S., Busecke, J.J., Cai, W.-J., Eyre, B.D., Forbrich, I., Kwon, E.Y., Maavara, T., 2023. Coastal vegetation and estuaries are collectively a greenhouse gas sink. Nat. Clim. Chang. 13 (6), 579–587.
Ruff, S.E., Kuhfuss, H., Wegener, G., Lott, C., Ramette, A., Wiedling, J., Knittel, K., Weber, M., 2016. Methane seep in shallow-water permeable sediment harbors high diversity of anaerobic methanotrophic communities, Elba, Italy. Front. Microbiol. 7, 374.
Rusch, A., Forster, S., Huettel, M., 2001. Bacteria, diatoms and detritus in an intertidal sandflat subject to advective transort across the water-sediment interface. Biogeochemistry 55, 1–27.
Saunois, M., Martinez, A., Poulter, B., Zhang, Z., Raymond, P.A., Regnier, P., Canadell, J. G., Jackson, R.B., Patra, P.K., Bousquet, P., 2025. Global methane budget 2000–2020. Earth Syst. Sci. Data 17 (5), 1873–1958.
Scheller, S., Yu, H., Ghadwick, G.L., McGlynn, S.E., Orphan, V.J., 2016. Artificial electron acceptors decouple archaeal methane oxidation from sulfate reduction. Science 351, 703–707.
Schnakenberg, A., Aromokeye, D.A., Kulkarni, A., Maier, L., Wunder, L.C., Richter-Heitmann, T., Pape, T., Ristova, P.P., Bühring, S.I., Dohrmann, I., 2021. Electron acceptor availability shapes anaerobically methane oxidizing archaea (ANME) communities in South Georgia sediments. Front. Microbiol. 12, 617280.
Schorn, S., Ahmerkamp, S., Bullock, E., Weber, M., Lott, C., Liebeke, M., Lavik, G., Kuypers, M.M., Graf, J.S., Milucka, J., 2022. Diverse methylotrophic methanogenic archaea cause high methane emissions from seagrass meadows. Proc. Natl. Acad. Sci. 119 (9), e2106628119.
Segarra, K.E., Comerford, C., Slaughter, J., Joye, S.B., 2013. Impact of electron acceptor availability on the anaerobic oxidation of methane in coastal freshwater and brackish wetland sediments. Geochim. Cosmochim. Acta 115, 15–30.
Smith, M.W., Davis, R.E., Youngblut, N.D., Kärnä, T., Herfort, L., Whitaker, R.J., Metcalf, W.W., Tebo, B.M., Baptista, A.M., Simon, H.M., 2015. Metagenomic evidence for reciprocal particle exchange between the mainstem estuary and lateral bay sediments of the lower Columbia River. Front. Microbiol. 6, 1074.
Smith, M.W., Herfort, L., Rivers, A.R., Simon, H.M., 2019. Genomic signatures for sedimentary microbial utilization of phytoplankton detritus in a fast-flowing estuary. Front. Microbiol. 10, 2475.
Sorokin, D.Y., Merkel, A.Y., Abbas, B., Makarova, K.S., Rijpstra, W.I.C., Koenen, M., Sinninghe Damsté, J.S., Galinski, E.A., Koonin, E.V., Van Loosdrecht, M.C., 2018. Methanonatronarchaeum thermophilum gen. nov., sp. nov. and'Candidatus Methanohalarchaeum thermophilum', extremely halo (natrono) philic methyl-reducing methanogens from hypersaline lakes comprising a new euryarchaeal class Methanonatronarchaeia classis nov. Int. J. Syst. Evol. Microbiol. 68 (7), 2199–2208.
Sun, J., Evans, P.N., Gagen, E.J., Woodcroft, B.J., Hedlund, B.P., Woyke, T., Hugenholtz, P., Rinke, C., 2021. Recoding of stop codons expands the metabolic potential of two novel Asgardarchaeota lineages. ISME Commun. 1 (1), 30.
Taubert, M., Grob, C., Howat, A.M., Burns, O.J., Pratscher, J., Jehmlich, N., von Bergen, M., Richnow, H.H., Chen, Y., Murrell, J.C., 2017. Methylamine as a nitrogen source for microorganisms from a coastal marine environment. Environ. Microbiol. 19 (6), 2246–2257.
Thauer, R.K., 1998. Biochemistry of methanogenesis: a tribute to Marjory Stephenson. Microbiology 144, 2377–2406.
Thureborn, P., Franzetti, A., Lundin, D., Sjöling, S., 2016. Reconstructing ecosystem functions of the active microbial community of the Baltic Sea oxygen depleted sediments. PeerJ 4, e1593.
Tilbrook, B.D., Karl, D.M., 1995. Methane sources, distributions and sinks from California coastal waters to the oligotrophic North Pacific gyre. Mar. Chem. 49 (1), 51–64.
Timmers, P.H.A., Welte, C.U., Koehorst, J.J., Plugge, C.M., Jetten, M.S.M., Stams, A.J.M., 2017. Reverse methanogenesis and respiration in methanotrophic archaea. Archaea Article ID 1654237.
Treude, T., Krüger, M., Boetius, A., Jørgensen, B.B., 2005. Environmental control on anaerobic oxidation of methane in the gassy sediments of Eckernförde Bay (German Baltic). Limnol. Oceanogr. 50, 1771–1786.
Valenzuela, E.I., Avendaño, K.A., Balagurusamy, N., Arriaga, S., Nieto-Delgado, C., Thalasso, F., Cervantes, F.J., 2019. Electron shuttling mediated by humic substances fuels anaerobic methane oxidation and carbon burial in wetland sediments. Sci. Total Environ. 650, 2674–2684.
Vizza, C., West, W.E., Jones, S.E., Hart, J.A., Lamberti, G.A., 2017. Regulators of coastal wetland methane production and responses to simulated global change. Biogeosciences 14 (2), 431–446.
Waite, D.W., Chuvochina, M., Pelikan, C., Parks, D.H., Yilmaz, P., Wagner, M., Loy, A., Naganuma, T., Nakai, R., Whitman, W.B., 2020. Proposal to reclassify the proteobacterial classes Deltaproteobacteria and Oligoflexia, and the phylum Thermodesulfobacteria into four phyla reflecting major functional capabilities. Int. J. Syst. Evol. Microbiol. 70 (11), 5972–6016.
Wallenius, A.J., Dalcin Martins, P., Slomp, C.P., Jetten, M.S., 2021. Anthropogenic and environmental constraints on the microbial methane cycle in coastal sediments. Front. Microbiol. 12, 631621.
Wang, X.-C., Lee, C., 1990. The distribution and adsorption behavior of aliphatic amines in marine and lacustrine sediments. Geochim. Cosmochim. Acta 54 (10), 2759–2774.
Wang, X.-C., Lee, C., 1993. Adsorption and desorption of aliphatic amines, amino acids and acetate by clay minerals and marine sediments. Mar. Chem. 44 (1), 1–23.
Wang, X.-C., Lee, C., 1994. Sources and distribution of aliphatic amines in salt marsh sediment. Org Geochem. 22 (6), 1005–1021.
Wang, Y., He, L., Liu, J., Arndt, K.A., Mazza Rodrigues, J.L., Zona, D., Lipson, D.A., Oechel, W.C., Ricciuto, D.M., Wullschleger, S.D., 2024. Intensified positive arctic–methane feedback under IPCC climate scenarios in the 21st century. Ecosyst. Health Sustainability 10, 0185.
Weber, K.A., Achenbach, L.A., Coates, J.D., 2006. Microorganisms pumping iron: anaerobic microbial iron oxidation and reduction. Nat. Rev. Microbiol. 4 (10), 752–764.
Wehrmann, L.M., Risgaard-Petersen, N., Schrum, H.N., Walsh, E.A., Huh, Y., Ikehara, M., Pierre, C., D'Hondt, S., Ferdelman, T.G., Ravelo, A.C., 2011. Coupled organic and inorganic carbon cycling in the deep subseafloor sediment of the northeastern Bering Sea Slope (IODP Exp. 323). Chem. Geol. 284 (3–4), 251–261.
Wei, S., Han, G., Chu, X., Song, W., He, W., Xia, J., Wu, H., 2020. Effect of tidal flooding on ecosystem CO_2 and CH_4 fluxes in a salt marsh in the Yellow River Delta. Estuar. Coast. Shelf Sci. 232, 106512.

Winfrey, M.R., Ward, D.M., 1983. Substrates for sulfate reduction and methane p roduction in i ntertidal sediments. Appl. Environm. Microbiol 45 (1), 193–199.
Xiao, K., Beulig, F., Roy, H., Jorgensen, B., Risgaard-Petersen, N., 2018. Methylotrophic methanogenesis fuels cryptic methane cycling in marine surface sediment. Limnol. Oceanogr. 63 (4), 1519–1527.
Xiao, K.-Q., Beulig, F., Kjeldsen, K.U., Jørgensen, B.B., Risgaard-Petersen, N., 2017. Concurrent methane production and oxidation in surface sediment from Aarhus Bay, Denmark. Front. Microbiol. 8.
Xiao, K.-Q., Moore, O.W., Babakhani, P., Curti, L., Peacock, C.L., 2022. Mineralogical control on methylotrophic methanogenesis and implications for cryptic methane cycling in marine surface sediment. Nat. Commun. 13 (1), 1–9.
Xu, C., Wong, V.N., Reef, R., 2021. Effect of inundation on greenhouse gas emissions from temperate coastal wetland soils with different vegetation types in southern Australia. Sci. Total Environ. 763, 142949.
Yan, Z., Du, K., Yan, Y., Huang, R., Zhu, F., Yuan, X., Wang, S., Ferry, J.G., 2023. Respiration-driven methanotrophic growth of diverse marine methanogens. P. Natl. Acad. Sci. USA 120 (39) e2303179120.
Yan, Z., Joshi, P., Gorski, C.A., Ferry, J.G., 2018. A biochemical framework for anaerobic oxidation of methane driven by Fe (III)-dependent respiration. Nat. Commun. 9 (1), 1642.
Young, C.M., 2003. Reproduction, development and life-history traits. In: Tyler, P.A. (Ed.), Deep-Sea Ecosystems. Elsevier, Amsterdam.
Yuan, J., Ding, W., Liu, D., Xiang, J., Lin, Y., 2014. Methane production potential and methanogenic archaea community dynamics along the Spartina alterniflora invasion chronosequence in a coastal salt marsh. Appl. Microbiol. Biotechnol. 98, 1817–1829.
Yuan, J., Liu, D., Ji, Y., Xiang, J., Lin, Y., Wu, M., Ding, W., 2019. Spartina alterniflora invasion drastically increases methane production potential by shifting methanogenesis from hydrogenotrophic to methylotrophic pathway in a coastal marsh. J. Ecol. 107 (5), 2436–2450.
Zemskaya, T., Bukin, S., Lomakina, A., Pavlova, O., 2021. Microorganisms in the sediments of Lake Baikal, the deepest and oldest lake in the world. Microbiology 90 (3), 298–313.
Zhao, M., Han, G., Li, J., Song, W., Qu, W., Eller, F., Wang, J., Jiang, C., 2020. Responses of soil CO_2 and CH_4 emissions to changing water table level in a coastal wetland. J. Clean. Prod. 269, 122316.
Zhao, Y., Liu, Y., Cao, S., Hao, Q., Liu, C., Li, Y., 2024. Anaerobic oxidation of methane driven by different electron acceptors: a review. Sci. Total Environ. 174287.
Zhuang, G.-C., Elling, F.J., Nigro, L.M., Samarkin, V., Joye, S.B., Teske, A., Hinrichs, K.-U., 2016. Multiple evidence for methylotrophic methanogenesis as the dominant methanogenic pathway in hypersaline sediments from the Orca Basin, Gulf of Mexico. Geochim. Cosmochim. Acta 187, 1–20.
Zhuang, G.-C., Heuer, V.B., Lazar, C.S., Goldhammer, T., Wendt, J., Samarkin, V.A., Elvert, M., Teske, A.P., Joye, S.B., Hinrichs, K.-U., 2018. Relative importance of methylotrophic methanogenesis in sediments of the Western Mediterranean Sea. Geochim. Cosmochim Acta 224.
Zhuang, G.-C., Lin, Y.-S., Bowles, M.W., Heuer, V.B., Lever, M.A., Elvert, M., Hinrichs, K.-U., 2017. Distribution and isotopic composition of trimethylamine, dimethylsulfide and dimethylsulfoniopropionate in marine sediments. Mar. Chem. 196, 35–46.
Zhuang, G.-C., Montgomery, A., Joye, S.B., 2019. Heterotrophic metabolism of C1 and C2 low molecular weight compounds in northern Gulf of Mexico sediments: controlling factors and implications for organic carbon degradation. Geochim. Cosmochim. Acta 247, 243–260.
Ziebis, W., Huettel, M., Forster, S., 1996. The impact of biogenic sediment topography on oxygen fluxes in permeable sediments. Mar. Ecol. Prog. Ser. 140, 227–237.